The Ca^{2+}-activated Cl^- channel TMEM16B regulates action potential firing and axonal targeting in olfactory sensory neurons

Gianluca Pietra,[1]* Michele Dibattista,[2]* Anna Menini,[1] Johannes Reisert,[2] and Anna Boccaccio[3]

[1]Neurobiology Group, International School for Advanced Studies (SISSA), 34136 Trieste, Italy
[2]Monell Chemical Senses Center, Philadelphia, PA 19104
[3]Institute of Biophysics, National Research Council (CNR), 16149 Genova, Italy

The Ca^{2+}-activated Cl^- channel TMEM16B is highly expressed in the cilia of olfactory sensory neurons (OSNs). Although a large portion of the odor-evoked transduction current is carried by Ca^{2+}-activated Cl^- channels, their role in olfaction is still controversial. A previous report (Billig et al. 2011. *Nat. Neurosci.* http://dx.doi.org/10.1038/nn.2821) showed that disruption of the *TMEM16b/Ano2* gene in mice abolished Ca^{2+}-activated Cl^- currents in OSNs but did not produce any major change in olfactory behavior. Here we readdress the role of TMEM16B in olfaction and show that TMEM16B knockout (KO) mice have behavioral deficits in odor-guided food-finding ability. Moreover, as the role of TMEM16B in action potential (AP) firing has not yet been studied, we use electrophysiological recording methods to measure the firing activity of OSNs. Suction electrode recordings from isolated olfactory neurons and on-cell loose-patch recordings from dendritic knobs of neurons in the olfactory epithelium show that randomly selected neurons from TMEM16B KO mice respond to stimulation with increased firing activity than those from wild-type (WT) mice. Because OSNs express different odorant receptors (ORs), we restrict variability by using a mouse line that expresses a GFP-tagged I7 OR, which is known to be activated by heptanal. In response to heptanal, we measure dramatic changes in the firing pattern of I7-expressing neurons from TMEM16B KO mice compared with WT: responses are prolonged and display a higher number of APs. Moreover, lack of TMEM16B causes a markedly reduced basal spiking activity in I7-expressing neurons, together with an alteration of axonal targeting to the olfactory bulb, leading to the appearance of supernumerary I7 glomeruli. Thus, TMEM16B controls AP firing and ensures correct glomerular targeting of OSNs expressing I7. Altogether, these results show that TMEM16B does have a relevant role in normal olfaction.

The Journal of General Physiology

INTRODUCTION

The olfactory system detects small volatile molecules, odorants, which enter the nasal cavity via the inhaled air during normal breathing or sniffing. Odorants bind to odorant receptors (ORs) located on the cilia of olfactory sensory neurons (OSNs). Each OSN expresses only one type of OR from ∼1,000 in the mouse genome. Cilia are embedded in the mucus covering the epithelium and are the site of olfactory transduction. Odorant molecules, once bound to ORs, activate a G protein–coupled transduction cascade by activating the olfactory G protein G_{olf}, which in turn activates adenylate cyclase III, leading to the production of cAMP and culminating in the opening of two types of ion channels, CNG and Ca^{2+}-activated Cl^- channels. CNG channels in the ciliary membrane of OSNs have been first described by Nakamura and Gold (1987), they are directly activated by cAMP, and they induce a depolarizing influx of Na^+ and Ca^{2+} ions (reviewed by Schild and Restrepo, 1998; Pifferi et al., 2006, 2010; Kleene, 2008).

The presence of a Ca^{2+}-activated Cl^- conductance was first demonstrated in the cilia of frog OSNs by Kleene and Gesteland (1991), which showed that a rise in intraciliary Ca^{2+} concentration directly activates an anion-selective current in the ciliary membrane. Subsequent studies showed that Ca^{2+}-activated Cl^- channels are present also in other species, including rodents, and that they are activated by Ca^{2+} entry through CNG channels producing a large secondary Cl^- current (Kleene and Gesteland, 1991; Kleene, 1993, 1997; Kurahashi and Yau, 1993; Lowe and Gold, 1993; Firestein and Shepherd, 1995; Zhainazarov and Ache, 1995; Reisert et al., 2005; Boccaccio and Menini, 2007). In electrophysiological recordings from OSNs isolated from rats or mice, Ca^{2+}-activated Cl^- currents (CaCCs) account for up to 90% of the transduction current (Lowe and Gold, 1993; Boccaccio and Menini, 2007). CaCCs are depolarizing currents as a result of the active Cl^- ions accumulation inside OSNs. This

*G. Pietra and M. Dibattista contributed equally to this paper.
Correspondence to Anna Boccaccio: boccaccio@ge.ibf.cnr.it; Anna Menini: menini@sissa.it; or Johannes Reisert: jreisert@monell.org
M. Dibattista's present address is Dept. of Basic Medical Sciences Neuroscience and Sensory Organs, University of Bari Aldo Moro, 70121 Bari, Italy.

Abbreviations used: ACSF, artificial cerebrospinal fluid; AP, action potential; CaCC, Ca^{2+}-activated Cl^- current; IBMX, 3-isobutyl-1-methylxanthine; IF, instantaneous frequency; ISI, interspike interval; KO, knockout; NFA, niflumic acid; OB, olfactory bulb; OR, odorant receptor; OSN, olfactory sensory neuron; PSTH, peristimulus time histogram.

The Rockefeller University Press $30.00
J. Gen. Physiol. 2016 Vol. 148 No. 4 293–311
www.jgp.org/cgi/doi/10.1085/jgp.201611622

process is mainly mediated by the Na^+-K^+-$2Cl^-$ cotransporter NKCC1, which elevates Cl^- inside the cilia up to the same range as the Cl^- concentration present in the embedding mucus (Reuter et al., 1998; Kaneko et al., 2004; Reisert et al., 2005; Nickell et al., 2006). Additionally, the presence of the excitatory Cl^- current steepens the dependence of the transduction current on the stimulus amplitude, contributing to narrowing the neuron's dynamic range (Lowe and Gold, 1993; Boccaccio et al., 2006; Kleene, 2008).

The transduction current elicited by odorants produces a depolarization leading to generation of action potentials (APs) that are conducted to the olfactory bulb (OB) along the OSN axon (reviewed by Schild and Restrepo, 1998). OSNs not only generate APs after odorant activation of the transduction current, but also fire APs in the absence of stimulation (O'Connell and Mozell, 1969; Trotier and MacLeod, 1983; Frings and Lindemann, 1991; Reisert and Matthews, 2001; Reisert, 2010). What is the origin of basal firing activity in OSNs? OSNs are intrinsically noisy as demonstrated by the current produced by the addition of the phosphodiesterase inhibitor 3-isobutyl-1-methylxanthine (IBMX) and as shown by variations in the baseline current in the absence of odorants (Lowe and Gold, 1995). By investigating the basal activity of OSNs expressing identified ORs in the absence of odorant stimulation, it has been shown that spontaneous firing in OSNs is driven by the constitutive activity of the expressed OR. For example, OSNs expressing the I7 or the M71 OR have higher rates of spontaneous activity than mOR-EG OSNs (Reisert, 2010; Connelly et al., 2013). The basal firing activity can be suppressed by odorants that function as inverse agonist (Reisert, 2010) or by expressing an inactive mutant of the I7 OR (Connelly et al., 2013). Therefore, in the absence of odorants, the origin of spontaneous firing of an OSN is the spontaneous activation of its expressed OR. It is of interest to note that recent work (Dibattista and Reisert, 2016) has demonstrated that olfactory marker protein (OMP) controls basal cAMP levels (as well as odorant-induced cAMP levels) in an OR-dependent manner, ensuring that the expressed OR is the main source of noise. Of course, in addition to spontaneous activation of ORs, spontaneous activation of ion channels other than the two transduction ion channels, e.g., voltage-gated channels, could contribute to basal firing. However, Reisert (2010) showed that spontaneous firing in OSNs expressing identified receptors is greatly suppressed by the addition of 300 µM niflumic acid (NFA), a well-known blocker of CaCCs (Kleene, 1993; see also Fig. 7 A of Dibattista and Reisert, 2016). Importantly, these results indicate that olfactory transduction and the Cl^- current contribute to the basal firing activity of OSNs (Reisert, 2010).

A change in spontaneous firing of OSNs expressing the same OR may have very important consequences at the level of the OB. Indeed, it is well known that not only all OSNs expressing the same OR send their axons to specific glomeruli in the OB, but also OSN spontaneous firing plays a critical role to establish and maintain a correct glomerular targeting (Yu et al., 2004; Lodovichi and Belluscio, 2012; Nakashima et al., 2013b,a; Lorenzon et al., 2015; Nishizumi and Sakano, 2015). Nakashima et al. (2013b) have shown that the intrinsic activity of ORs, in the absence of odorants, influences the targeting of olfactory axon. Indeed, they showed that altered basal activity produces different levels of axon guidance molecules whose expression is dependent on the basal cAMP level (Imai et al., 2006; Nakashima et al., 2013b).

Interestingly, although CaCCs were first observed in the early nineties (Kleene and Gesteland, 1991; Kleene, 1993; Kurahashi and Yau, 1993; Lowe and Gold, 1993), their molecular identity has been elusive for over two decades, hindering the possibility to better understand the role of CaCCs in the olfactory system. After ruling out several possible candidates, the channels expressed in OSN cilia responsible for CaCCs were finally identified as TMEM16B/Anoctamin2 (Pifferi et al., 2009, 2012; Stephan et al., 2009; Sagheddu et al., 2010; Billig et al., 2011), a member of the *Tmem16* (*Anoctamin*) gene family (Pedemonte and Galietta, 2014). Disruption of the *TMEM16b* (*Ano2*) gene in mice (Billig et al., 2011) completely abolished CaCCs in OSNs. However, TMEM16B knockout (KO) mice were reported not to have any obvious olfactory deficit, leading to the conclusion that CaCCs are dispensable for olfaction and suggesting that odorant-evoked CNG currents, which remain in OSNs of TMEM16B KO mice, are sufficient to encode odorant information and support near-normal olfactory function (Billig et al., 2011). As this first (and until now only) study on TMEM16B KO mice raised serious doubts about a relevant role of Ca^{2+}-activated Cl^- channels in olfaction (Billig et al., 2011), we sought to reexamine this question by further extending the experimental analysis and comparing additional aspects of olfactory function in TMEM16B KO versus WT mice.

As the role of TMEM16B in OSN firing has not been investigated yet, we measured both spontaneous and stimulus-induced firing activity. We found a decrease in spontaneous firing activity in randomly chosen OSNs in TMEM16B KO compared with WT mice. To reduce the variability caused by the expression of different ORs in randomly chosen OSNs, we analyzed firing activity of OSNs expressing the I7 OR. To identify I7 OSNs, we used I7-IRES-tauGFP (Bozza et al., 2002) mice crossed with TMEM16B KO mice. In I7 OSNs, we measured a reduction of spontaneous firing activity in the absence of TMEM16B compared with control mice. Moreover, we identified a dramatic change in the firing pattern in response to heptanal, a well-known agonist for the I7 OR.

This change was manifested as a prolonged odorant response and a higher number of APs per response in I7 OSNs from TMEM16B KO compared with WT mice. Axonal targeting of I7 OSNs to the OB was also altered, as indicated by the presence of supernumerary I7 glomeruli in TMEM16B KO mice. Furthermore, from a behavioral point of view, TMEM16B KO mice showed a reduction in the ability to use olfactory cues to locate previously unknown buried food compared with WT mice. Our results demonstrate that the Ca^{2+}-activated Cl^- channel plays a physiological role in olfaction, showing that it is not simply dispensable for all aspects of olfaction, but it is required for certain olfactory-driven behaviors. Moreover, in contrast to previous findings showing normal axonal targeting of OSNs expressing the P2 or M72 ORs (Billig et al., 2011), we find that axons of I7-expressing OSNs target an abnormally large number of glomeruli in the OB. Importantly, TMEM16B had an influence on OSN AP firing rates.

MATERIALS AND METHODS

Animals

Mice were handled in accordance with the guidelines of the Italian Animal Welfare Act and European Union guidelines on animal research, under a protocol approved by the ethic committee of SISSA or in accordance with methods approved by the Animal Care and Use Committees of the Monell Chemical Senses Center (conforming to National Institutes of Health guidelines).

In this study we used TMEM16B KO and WT mice derived from breeder pairs provided by T. Jentsch (Leibniz-Institut für Molekulare Pharmakologie/Max-Delbrück-Centrum für Molekulare Medizin, Berlin, Germany; Billig et al., 2011). To record from OSNs expressing an identified OR and for immunohistological experiments, TMEM16B KO mice were crossed with I7-IRES-tauGFP, a mouse line in which OSNs expressing the I7 OR also expressed GFP (Bozza et al., 2002) with control mice obtained from the I7-IRES-tauGFP mouse line. The I7-IRES-tauGFP mouse strain was a gift from P. Mombaerts (Max Planck Research Unit for Neurogenetics, Frankfurt, Germany).

Odor-guided food seeking test

A small piece of food was buried below the surface of the cage bedding so that it constituted a purely olfactory cue, and the time taken by a mouse to find the food item was recorded. All mice of either sex were maintained on a 12:12 light/dark cycle and tested in the light phase in the Monell Chemical Senses Center animal facility where temperature and humidity were kept at 23°C and 45%, respectively. Mice were food deprived overnight with ad libitum access to water. Every morning, each mouse was placed in a novel test cage (standard mouse cage, L * H * W, 24 cm * 12 cm * 15 cm) in which an ∼3-g piece of cookie (Oreo; Nabisco) had been buried under fresh bedding. The latency of the animal to retrieve the cookie was recorded with a stopwatch and by an experimenter that was blinded to the animal's genotype. Retrieving the cookie was defined as digging it up with forepaws, picking it up, and placing it in the mouth. We set a 10-min limit within which the animals had to find the cookie; after that, the time was stopped and the cookie was exposed so that the mouse could have access to and eat it. The position of the buried cookie was randomly changed every day so that the animal could not rely on spatial information to find it. This was repeated for 5 d. Mice were weighed every morning before experiments to monitor their body weight. 1.5 g of standard chow (Tekland rodent diet 8604) was given every day after testing to maintain body weight. If a mouse was found to have <80% starting body weight, additional food was given to maintain a healthy body weight. On the sixth day, the cookie was placed on top of the bedding. We repeated this same type of experiment with a second set of mice and cheese (Cracker Barrel extra sharp cheddar cheese stick; Kraft) that had been buried under fresh bedding. If a mouse could not find the cheese within 10 min, the test was terminated and the latency was recorded as 600 s.

Mice were returned to normal food for 1 wk. After 1 wk, mice were again food deprived overnight, and the following five food items were hidden in the bedding over the next 5 d, one food was tested each day: cookie (Oreo), peanut (select whole peanuts in shell, deshelled), cheese (Cracker Barrel extra sharp cheddar cheese stick), chocolate (Hershey's milk chocolate king size), and standard chow. The time the mice took to retrieve the food was recorded, and the limit to perform the task was 15 min. The second set of mice that had previously performed the cheese-seeking task were exposed, after a week of rest, to cheese, peanut, cookie, chocolate, and standard chow hidden in the bedding over the next 5 d; one food was tested each day.

Preparation of dissociated OSNs

Mice (3–5 wk of either sex) were anesthetized with CO_2 inhalation and decapitated, and the head was hemisected sagittally along the septum. The olfactory epithelium was removed, and OSNs were dissociated either mechanically for suction pipette recordings (Ponissery Saidu et al., 2012) or enzymatically, with a papain–cysteine treatment, for uncaging patch-clamp experiments (Lagostena and Menini, 2003; Boccaccio et al., 2006, 2011).

Patch-clamp experiments and photorelease of caged 8-Br-cAMP

Currents were measured from dissociated OSNs with an Axopatch 200B patch-clamp amplifier (Axon Instruments) in the whole-cell voltage-clamp mode.

For flash photolysis, we used a xenon flash-lamp system JML-C2 (Rapp OptoElectronic) coupled into the epifluorescence port of the microscope with a quartz light guide (Boccaccio et al., 2006, 2011). The spot of light had a diameter of ∼15 µm that could cover only the ciliary region and, in some cases, also part of the dendrite. The flash duration was 1.5 ms. We used [6,7-Bis(carboxymethoxy)coumarin-4-yl]methyl-8-bromoadenosine-3′, 5′-cyclic monophosphate (BCMCM-caged 8-Br-cAMP; Boccaccio et al., 2006), dissolved in DMSO at 10 mM and added to the intracellular solution at a final concentration of 50 µM. The compound was a gift from V. Hagen (Leibniz-Institut für Molekulare Pharmakologie).

Patch pipettes were pulled from borosilicate glass and filled with the intracellular solution containing (mM) 140 KCl, 4 $MgCl_2$, 0.5 EGTA, and 10 HEPES, pH 7.4, and additionally 50 µM BCMCM-caged 8-Br-cAMP. Bath mammalian Ringer solution contained (mM) 140 NaCl, 5 KCl, 1 $CaCl_2$, 1 $MgCl_2$, 10 HEPES, 10 glucose, and 1 Na-pyruvate, pH 7.4. All experiments were performed at room temperature (20–22°C).

Suction pipette recordings

Recordings from isolated OSNs were made using the suction pipette technique as described previously (Lowe and Gold, 1991; Ponissery Saidu et al., 2012). In brief, a freshly dissociated OSN was gently drawn inside the tip of the recording pipette so that its knob and cilia remained exposed to bath and/or stimulus solutions. In this recording configuration, the intracellular voltage is free to vary and APs are recorded as fast biphasic transients. The recorded suction current was filtered at DC −5,000 Hz (−3 dB, 8-pole Bessel filter) to display the fast APs, and the underlying receptor current was isolated by low-pass filtering at 50 Hz (−3 dB, 8-pole Bessel filter). The recorded suction current was sampled at 10 kHz. Currents were recorded with a Warner PC-501A patch clamp amplifier, digitized using Power1401 II A/D converter and Signal acquisition software (Cambridge Electronic Design).

Solutions and solution exchange in the suction experiments

Mammalian Ringer's solution contained (mM) 140 NaCl, 5 KCl, 1 $MgCl_2$, 2 $CaCl_2$, 0.01 EDTA, 10 HEPES, and 10 glucose. The pH was adjusted to 7.5 with NaOH. NFA and IBMX were used at concentrations of 300 µM and 1 mM, respectively, by dissolving them directly into Ringer's without the use of DMSO.

Fast solution changes and odorant exposures were achieved by transferring the tip of the recording pipette containing the OSN across the interface of neighboring streams of solutions using the Perfusion Fast-Step solution changer (Warner Instrument Corporation). All experiments were performed at mammalian body temperature (37°C). Solutions were heated just before entering the solution changer by a solution heater based on Matthews (1999).

Intact mouse olfactory epithelium preparation

Mice (4–12 wk) were anesthetized with CO_2 inhalation and decapitated, and the head was immediately transferred to ice-cold artificial cerebrospinal fluid (ACSF) bubbled with 95% O_2 and 5% CO_2. ACSF contained (mM) 120 NaCl, 5 KCl, 1 $MgSO_4$, 1 $CaCl_2$, 25 $NaHCO_3$, 10 glucose, and 10 HEPES, osmolarity before oxygenation was 310 mOsm, pH 7.2. The nasal septum was dissected en bloc, and the bone with the two attached epithelia was placed in a recording chamber at room temperature (21–24°C) that was continually perfused by bubbled ACSF.

Mouse nose coronal slice preparation

Coronal slices were prepared from olfactory epithelia of mouse pups (P0–P4). Mice were directly decapitated, and the nose was dissected en bloc and glued into a small hole in a cube of boiled carrot. A vibratome was used to cut coronal slices of 300-µm thickness. During the cutting, the tissue was completely submerged in ACSF continually oxygenated and kept near 0°C. After sectioning, coronal slices were allowed to recover for at least 30 min in ACSF continually oxygenated and kept near 0°C.

Loose-patch extracellular recordings

Dendritic knobs of individual OSNs in the olfactory epithelium were visualized using an upright microscope (BX51WI; Olympus) equipped with infrared differential contrast optics, a camera (DFK 72BUC02; Imaging Source) and a 40× water-immersion objective with an additional 2× auxiliary lens.

Extracellular recordings from dendritic knobs of OSNs in the intact olfactory epithelium were obtained in the loose-patch configuration with seal resistances of 20–40 MΩ (Nunemaker et al., 2003; Delay and Restrepo, 2004) in both coronal slices and intact olfactory epithelia preparations. Pipette solution was ACSF, as the bath solution, and the recordings were made in voltage-clamp mode with a holding potential of 0 mV. Data were low-pass filtered at 1 kHz and sampled at 5 kHz.

The experiments were performed at room temperature (21–24°C) using a MultiClamp 700B amplifier controlled by Clampex 9.2 via a Digidata 1322A (Molecular Devices). Patch pipettes were pulled from borosilicate capillaries (WPI) with a Narishige PC-10 puller and had resistances of 5–10 MΩ. OSNs expressing the I7 OR were stimulated by adding 500 µM heptanal to ACSF, one of the main ligands of I7 receptor (Krautwurst et al., 1998; Hall et al., 2004). Heptanal was dissolved at 100 mM in DMSO and stored at −20°C.

IBMX was prepared in a 20 mM stock solution containing 5% DMSO and diluted to the final concentration of 100 µM before use.

The stimulus, either odorant or IBMX, was delivered through a pipette by pressure ejection (10–15 psi) using a Picospritzer II (Parker). Stimulation delivering was visually controlled by adding fluorescein to the odorant solution. The stimulation intensity was modulated changing the puff duration. The stimulation pipette was placed at least 20 µm from the recorded OSN to avoid any mechanical response (Grosmaitre et al., 2007).

Data analysis of loose-patch extracellular recordings

Spontaneous firing activity was characterized from mean and instantaneous firing frequencies evaluated in a time window of 2–5 min. Mean spontaneous firing frequency was calculated as the number of spikes divided by the duration of the recording, and the instantaneous firing frequency as the inverse of the interspike interval (ISI) between consecutive spikes (second to first, third to second, and so forth). Sometimes very high-frequency spontaneous firing activity followed by complete silencing of the recorded OSN showed clear evidence of neural damage or loss of cell integrity; such units were routinely discarded. For spike detection, the raw data were filtered 2–1,000 Hz.

Odorant-evoked firing activity was detected on top of the spontaneous background activity using an established protocol for OSN response analysis (Rospars et al., 2003; Savigner et al., 2009; Lorenzon et al., 2015). In brief, neuronal spiking activity was defined as a presumptive response to odorant when, within 1.25 s after stimulus presentation, at least three consecutive spikes presented an instantaneous frequency (IF; 1/ISI) higher than the mean IF plus 1.5 Hz in the 30 s before stimulation (IF > avgIF + 1.5 Hz). If a presumptive response was detected, its instantaneous firing frequency distribution was compared using the Mann-Whitney *U* test with the instantaneous firing frequency distribution occurring before stimulation. When the two distributions were found significantly different at a level of 1%, the presumptive response was considered a true response, otherwise it was discarded.

Strong stimulations often produced a marked increment in firing frequency correlated with a progressive decrease of the AP amplitude. We defined a response as saturating when it was composed by APs that decreased their amplitude up to baseline, producing a silencing period that sometimes was followed by a high-frequency burst. During the rebound burst, the amplitude of APs increased and the frequency progressively decreased toward the spontaneous firing activity level (similarly to Rospars et al. [2003] and Savigner et al. [2009]).

To construct the normalized cumulative response (peristimulus time histogram [PSTH]), we summed single responses obtained from several cells stimulated with an identical stimulus. We optimized the bin size by calculating a cost function, according to Shimazaki and Shinomoto (2007). To analyze the difference between PSTHs from KO and WT cells, we applied the statistical procedure reported by Dörrscheidt (1981), with the null hypothesis that the two PSTHs derive from the same group of neurons and they consequently have the same firing rate.

The firing rate of the odorant-evoked response was estimated as an ISI of the first four spikes (Rospars et al., 2003). Moreover, the response intensity was visualized by a cumulative spike distribution histogram normalized by the number of responses, and it was quantified measuring the total number of spikes in the response and its duration. For saturating responses, the response duration referred to the time between the first and last spike recognized as part of the response, including the silent period and the firing rebound.

Data in Figs. 5, 6, 7, and 8 are presented as mean value and boxplots in which the inner square represents the mean, lines represent the median, upper and lower box boundaries represent the 25th and 75th percentile, and upper and lower whiskers represent the 5th and 95th percentiles. Spontaneous and evoked firing frequency data were not in all cases normally distributed (Kolmogorov-Smirnov test or Shapiro-Wilkinson test), and statistical significance was determined using Mann-Whitney *U* test. P-values <0.05 were considered statistically significant.

Perforated patch recordings

Perforated patch clamp recordings were performed on the dendritic knobs of OSNs from the epithelia attached to the septal bone (Ma et al., 1999; Jarriault and Grosmaitre, 2015).

Patch pipettes (9–18 MΩ) included 160 µM nystatin and were filled with the following solution (mM): 70 KCl, 53 KOH, 30 methane sulfonic acid, 5 EGTA, 10 HEPES, and 70 sucrose; osmolarity 300 mOsM; pH 7.2. The tip of the pipette was first filled with a nystatin-free solution. The solution containing the antibiotic to fill the patch pipettes was changed every 2 h, stored on ice, and protected from light. The measured junction potential was ∼7.5 mV and was corrected offline.

OB histochemistry

Mice (2–4 mo old) were sacrificed by cervical dislocation and decapitated, the head was immediately transferred to ice-cold ACSF solution, and the OBs were extracted. The fresh tissue was left overnight in a solution of 4% of paraformaldehyde (PFA) diluted in PBS. After the fixation, it was placed in 30% (wt/vol) sucrose and left overnight at 4°C for cryoprotection. 16-µm-thick sagittal sections were cut on a cryostat and stored at −20°C. Tissue sections washed in 0.1% (vol/vol) Tween 20 in PBS 30 min and rinsed with water. OB sections were incubated for 30 min with 4′-6-Diamidino-2-phenylindole (DAPI; 0.1 µg/ml) to reveal cell nuclei. Tissue sections were then washed and mounted

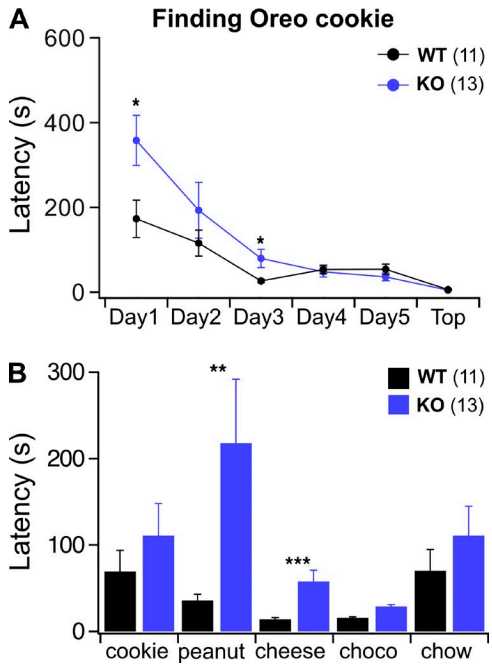

Figure 1. **Behavioral deficits in TMEM16B KO mice.** (A) WT and KO mice had to locate an Oreo cookie buried in the bedding of their cage. Experiments were performed once a day over 5 d, and on the sixth day the cookie was placed on top of the bedding. (B) After 1 wk on normal diet, the same mice were exposed to a series of odors that were known (Oreo and chow) or novel (peanut, cheese, or chocolate) to them. Mann-Whitney *U* test: *, $P < 0.05$; **, $P < 0.01$; ***, $P < 0.001$. Mean ± SEM from 11 WT and 13 KO mice.

with Vectashield (Vector Laboratories). Images were taken with an SP2 confocal microscope (Leica Microsystems) at a resolution of 1,024 × 1,024 pixels. Contrast and brightness of the images in Fig. 9 were manipulated with ImageJ software (National Institutes of Health) for the purpose of display only. Sectioning, staining, and glomerular counting were performed by an experimenter who was blinded to the genotype of the mice.

Chemicals

All compounds and chemicals were obtained from Sigma-Aldrich, unless otherwise stated.

RESULTS

TMEM16B KO mice display altered olfactory ability in finding buried food

We used an odor-guided food-seeking test where mice have to use their olfactory ability to locate a food item buried under the bedding chips in the cage. We ran the test for a consecutive 5 d. On the first day of testing, when mice were naive with respect to the food item and its odor (a piece of Oreo cookie), we observed that close to a fourth of TMEM16B KO mice (3 out of 13) failed to locate the food within the 10-min test time, whereas none of the WT exceeded 10 min. On average, KO mice were significantly slower in locating the cookie (Fig. 1 A; Mann-Whitney *U* test, $P < 0.05$). During the following 4 d of testing, both WT and KO mice began to locate the food faster, and in the end, KO mice could perform the task as quickly as WT. TMEM16B KO mice did not show any gross motor, metabolic, or motivational deficits as they performed equally well as WT mice when the food was presented visually on top of the bedding and not buried underneath it (Fig. 1 A).

Because the differences between TMEM16B KO and WT mice were prominent on the very first day of the experiment, we hypothesized that KO mice may not be able to reliably recognize new odors. We tested this hypothesis by giving the animals a week of rest and recovery and after the eighth day of testing exposed them daily to new sources of odors (and new kind of food). On the first day of this second set of experiments, mice were challenged to retrieve the same known kind of cookie used in the first set, and both WT and KO performed equally (Fig. 1 B). This suggests that mice retained the effect of the previous sessions of experiments and the identity of the odor. Over the following 2 d, peanut or cheese was buried, and TMEM16B KO mice displayed greater latencies in locating the source of the odor. Indeed, in both cases, KO mice were around twofold slower than WT. These results confirm that, even when the task was already known, KO mice did not locate the food as fast as WT when exposed to new food odors (Fig. 1 B; Mann-Whitney *U* test, peanut $0.001 < P < 0.01$ and cheese $P < 0.001$). When challenged to find chocolate (Fig. 1 B), both strains performed equally fast, even though we observed a tendency for the KO to perform slower than the WT. Possibly a "floor" effect occurred, diminishing the difference between WT and KO mice. It is also possible that mice used cocoa, which is also present in the cookie, to locate the source of odor, thus making chocolate not an entirely new odor. The last day of the experiment mice had to locate a familiar source of odor (and food), their standard chow, and differences between WT and KO vanished. Also, with a new and naive set of mice we repeated the same type of experiments, but this time we used cheese as the food item to be found for the first consecutive 5 d. Again, KO mice were significantly slower to locate the cheese on the first 2 d but were equally fast for the remaining 3 d. After 1 wk of rest, we tested the new cohort of mice for their ability to locate new sources of odor. Now WT and KO mice could locate the cheese equally fast, but KO mice performed significantly slower on the now new cookie odor. Altogether, these experiments suggest that TMEM16B KO have deficits in recognizing or locating the source of some odors that are novel to them.

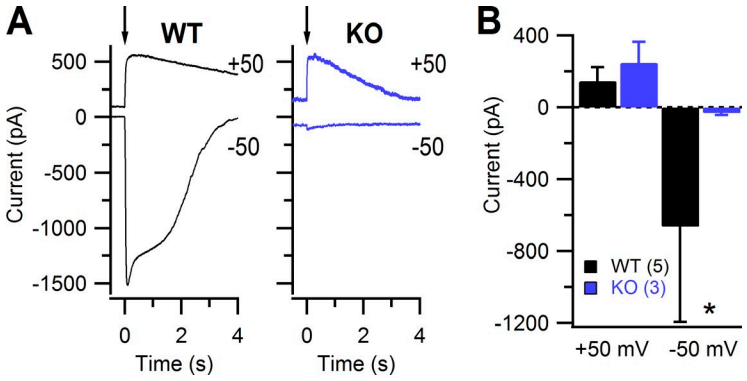

Figure 2. **Transduction current elicited by 8-Br-cAMP photorelease recorded in isolated olfactory neurons.** (A) Representative whole cell response to photorelease of 8-Br-cAMP at a holding potential of −50 mV and 50 mV for WT and KO OSNs. The arrows indicate the time of application of UV light flashes. (B) Summary of the mean maximal current ± SD. n = 5 from 4 WT mice; n = 3 from 2 KO mice; Mann-Whitney U test: *, P < 0.05.

CaCCs are absent in OSNs from TMEM16B KO mice

Given the olfactory deficits we observed, we focused on comparing the electrophysiological properties of OSNs in the absence and in the presence of TMEM16B. First, similar to experiments previously reported for OSNs in tissue slices (Billig et al., 2011), we investigated Cl^- currents in OSNs isolated from WT and TMEM16B KO mice using flash photolysis of caged 8-Br-cAMP combined with patch-clamp recordings, a technique we used extensively to characterize transduction currents in isolated OSNs (Boccaccio et al., 2006; Boccaccio and Menini, 2007). We used caged 8-Br-cAMP instead of caged cAMP because 8-Br-cAMP is a potent agonist of the olfactory CNG channel and therefore permits a more robust activation of the transduction cascade. We measured the whole-cell patch-clamp current evoked by photorelease of 8-Br-cAMP inside the cilia knob region of OSNs at various holding potentials (Fig. 2). At 50 mV, the current is mainly caused by the cationic efflux through CNG channels directly activated by 8-Br-cAMP. As little Ca^{2+} enters the cilia at 50 mV, only a small or negligible Cl^- current and/or Ca^{2+}-activated K^+ currents were activated. In contrast, at −50 mV, the influx of Ca^{2+} through CNG channels activated a large secondary CaCC (Fig. 2 A). Previous work has shown that the secondary large current at −50 mV was blocked by NFA, indicating that it was a CaCC (see Fig. 6 in Boccaccio and Menini, 2007). OSNs from TMEM16B KO did not show the secondary large component at −50 mV, whereas they retained a similar outward current amplitude at 50 mV (Fig. 2 A). Indeed, mean values for current amplitudes in WT and KO neurons were significantly different at −50 mV (Mann-Whitney U test, 0.01 < P < 0.05) but not at 50 mV (Fig. 2 B). Thus, we confirmed that CaCCs are absent in isolated OSNs from TMEM16B KO mice as previously shown by flash photolysis of caged Ca^{2+} and caged 8-Br-cAMP (Billig et al., 2011). As stated previously (Billig et al., 2011), the small residual current in KO OSNs at −50 mV was likely caused by CNG cationic currents, further demonstrating that in isolated OSNs the transduction current is largely carried by CaCCs through TMEM16B channels (Billig et al., 2011).

We also investigated the contribution of CaCCs to stimulus-induced responses using the suction pipette technique in isolated OSNs (Fig. 3). We stimulated OSNs with the phosphodiesterase inhibitor IBMX, a feasible alternative to odorant stimulation, as OSNs can have a high intrinsic activity (Reisert et al., 2007). Currents elicited by 1 mM IBMX (1-s application) were greatly reduced by application of the Cl^- current blocker NFA (300 µM) in WT OSNs (Fig. 3, A, C, and D). In OSNs from TMEM16B KO mice, IBMX application produced a significantly smaller current in KO compared with WT mice (Fig. 3, B and C). This small current could not be further reduced by the application of NFA (Fig. 3, B–D), a result consistent with the presence of a residual CNG current.

IBMX-evoked firing in OSNs

The OSN transduction current evoked by a stimulus (e.g., IBMX or odorants) produces a depolarization that elicits APs, which are sent to the OB along the OSN axon. Up to now, AP firing of TMEM16B KO OSNs has not been investigated.

We compared resting potential and input resistance of OSNs from TMEM16B WT and KO mice with nystatin-perforated patch experiments recorded from the dendritic knobs from OSNs located in the septal olfactory epithelium from adult mice. The mean resting potential, evaluated in current clamp at I = 0, was −77.5 ± 3.4 mV (mean ± SEM, n = 14) for WT and −79.1 ± 5.0 (mean ± SEM, n = 9) for KO mice (unpaired t test, P = 0.78). The input resistance was 3.8 ± 0.99 GΩ and 3.1 ± 0.57 GΩ (mean ± SEM, n = 5), respectively, for WT and KO mice (unpaired t test, P = 0.52). Input resistance was calculated as the ratio between the membrane potential change and the injected hyperpolarizing current.

In a first set of experiments, we compared AP firing in isolated OSNs from WT and KO mice stimulated by 1-s application of 1 mM IBMX using suction electrode recordings. In this recording configuration, both transduction current and APs, which are generated as the voltage is free to vary, can be simultaneously recorded using a large bandwidth filter setting (see Materials and methods). In WT OSNs, we recorded AP firing during

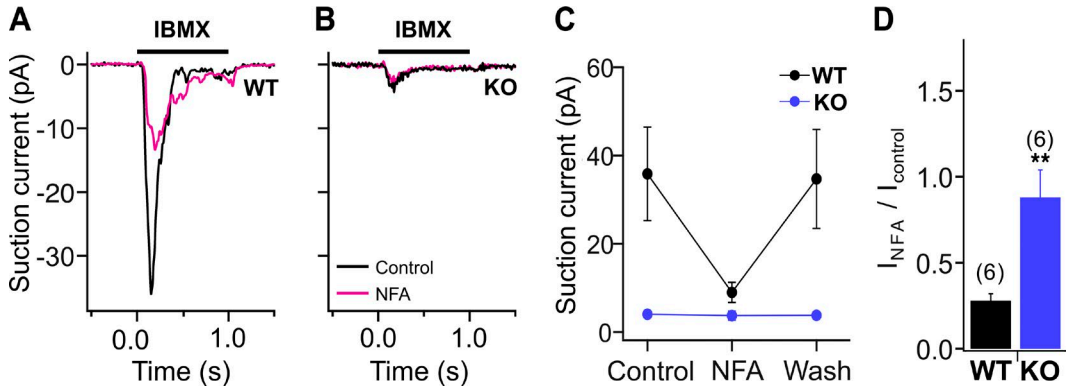

Figure 3. **Transduction current recorded with the suction pipette technique from isolated OSNs.** (A and B) Single-cell suction electrode recordings from a dissociated WT (A) and KO (B) OSN stimulated with a 1-s pulse of 1 mM IBMX in Ringer's solution and in the presence or absence of 300 µM NFA, a Cl^- channel blocker. (C and D) Suction peak currents measured in control, in the presence of NFA and after washout (C) and ratio of the response in the presence and absence of NFA (D). Mean ± SEM, $n = 6$ for WT and KO. Unpaired t test: **, $P < 0.01$.

the early rising phase of the IBMX-stimulated transduction current (Fig. 4 A). Surprisingly, TMEM16B KO OSNs fired APs during the entire IBMX transduction current (Fig. 4 B). On average, the number of spikes was significantly higher, and the spike train duration (measured as the time from the first to the last spike of the train to occur) was significantly longer in TMEM16B KO compared with WT mice (Fig. 4, A and B [insets], C, and D). Other parameters, such as the delay of the first AP (Fig. 4 E) and the maximal firing frequency (Fig. 4 F) were not significantly different in KO and WT mice. These results show that the lack of CaCCs altered the firing behavior in response to IBMX by increasing the number of spikes and prolonging the duration of the spike train in isolated OSNs from TMEM16B KO mice.

In a second set of experiments, we recorded from OSNs in situ by using an intact olfactory epithelium preparation instead of dissociated OSNs. In this preparation, OSNs still retain a large portion of their axons and are surrounded by a more physiological environment, including supporting cells. We recorded responses to IBMX using the loose-patch configuration from the dendritic knobs of OSNs. Fig. 5 A shows representative responses to a 50-ms puff of 100 µM IBMX of

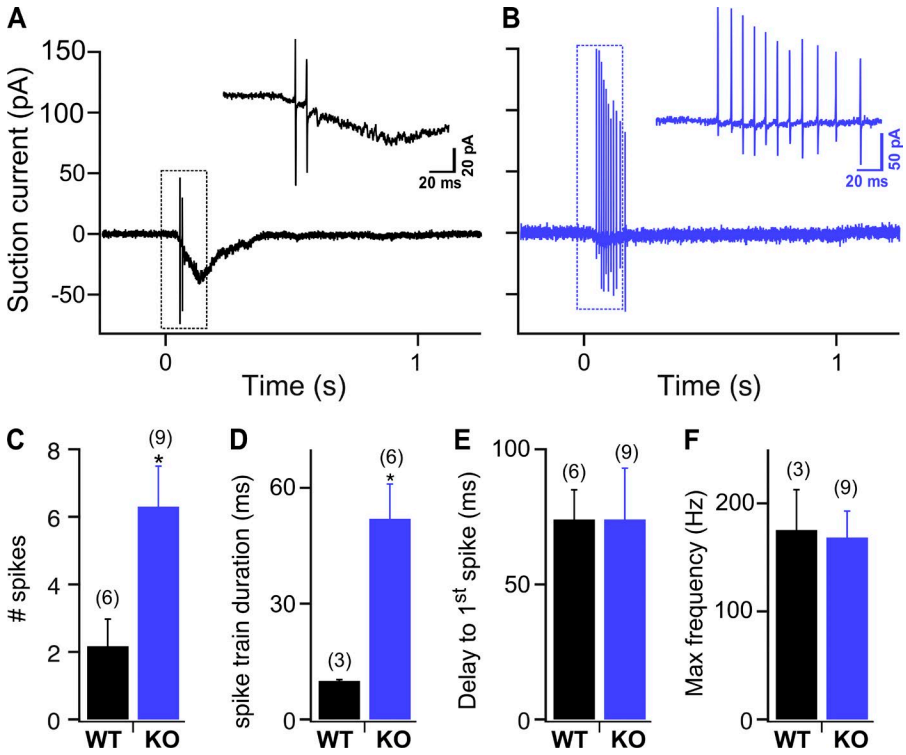

Figure 4. **Evoked activity recorded with the suction pipette technique in OSNs from WT and KO mice.** (A and B) Single-cell suction electrode recordings from a dissociated WT (A) and KO (B) OSN stimulated with a 1-s pulse of 1 mM IBMX. Insets show responses on an expanded time scale. The recording bandwidth was 0–5,000 Hz to display APs. (C–F) Differences in the response were quantified for the number of spikes (C), the duration of the train of elicited spikes (D), the delay of the first spike (E), and maximal firing frequency (F). Mean ± SEM; number of experiments is indicated in parentheses. Unpaired t test: *, $0.01 < P < 0.05$.

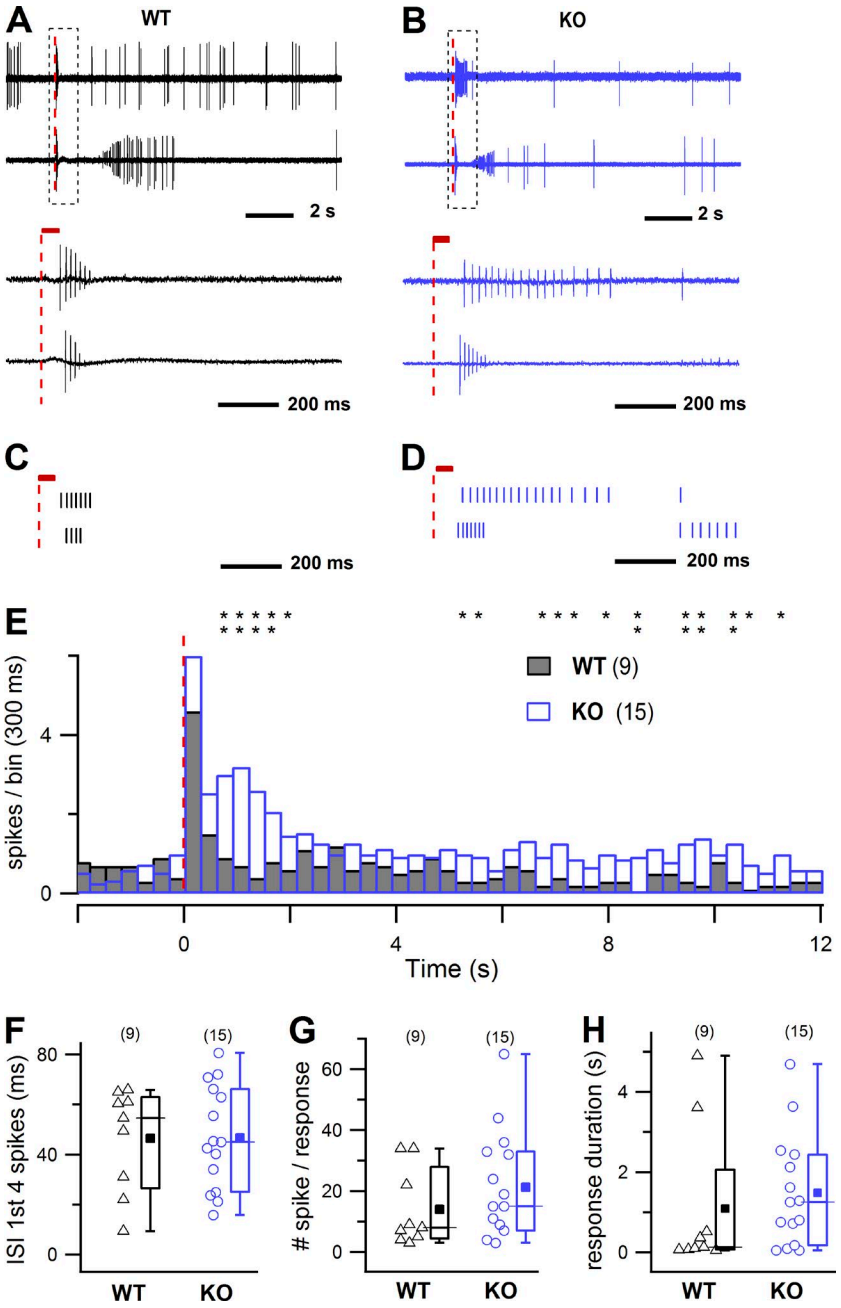

Figure 5. **Evoked activity in WT and KO OSNs.** (A and B) Representative responses to 100 µM IBMX stimulation (50 ms) for two different OSNs from WT (A) and KO mice (B). Data represent loose-patch recordings from dendritic knobs of OSNs located in the septum. The bottom panels show the regions enclosed by the dashed boxes on an expanded time scale. Broken red lines represent the onset of IBMX stimulation, and the red bars in the bottom panels its duration. (C and D) Raster plots on an enlarged time scale for the same cells shown in A and B. (E) Averaged responses to IBMX as in A and B, normalized to the number of neurons (n = 9 from 7 WT mice, n = 15 from 8 KO mice; bin 300 ms). The broken red line represents the onset of stimulation, and data belong to WT and KO PSTH distributions. *, 0.01 < P < 0.05; and **, P < 0.01. (F–H) Scatter and boxplots of ISI of the first four spikes (F; 47 ± 21 ms in WT, 47 ± 21 ms in KO), of the total number of spikes (G; 14 ± 13 spike/response in WT, 21 ± 18 spike/response in KO), and of the response duration (H; 1.1 ± 1.8 s in WT, 1.5 ± 1.4 s in KO; mean ± SD). In the box plots the squares represent the mean, lines represent the median, upper and lower box boundaries represent the 25th and 75th percentile, and upper and lower whiskers represent the 5th and 95th percentiles. Data were not statistically different (one-tail t test for data in F; Mann-Whitney U test, one tail, P > 0.05 for data in G and H). The number of experiments is indicated in parentheses.

two OSNs from WT mice. The IBMX responses of both OSNs consisted of an initial burst of APs of rapidly declining amplitude followed by a silent period (Fig. 5 A, bottom traces). The amplitude of the spikes progressively recovered after the silent time or spikes reappeared at full magnitude (Fig. 5 A, traces at the top) as previously described (Trotier, 1994, 1998; Duchamp-Viret et al., 2000; Reisert and Matthews, 2001; Savigner et al., 2009; Connelly et al., 2013; Lorenzon et al., 2015). Overall, the responses to IBMX of OSNs from KO mice had broadly similar properties to WT OSNs, with a spike burst, silent period, and spike reappearance, as illustrated by two representative KO OSNs (Fig. 5 B). The comparison between the cumulative responses normalized to the number of neurons (multicell PSTH; Fig. 5 E) shows the presence of a second broad peak in KO OSNs, indicating an increase in firing activity compared with WT OSNs. The asterisks in Fig. 5 E represent the bins with significantly higher firing rates in KO with respect to WT OSNs (analysis according to Dörrscheidt [1981]).

To quantitatively characterize the responses, we calculated the ISI of the first four spikes (Fig. 5 F), the total number of spikes in the response (Fig. 5 G), and the response duration (Fig. 5 H). Although the PSTH distribution differed between KO and WT mice, these parameters were not significantly different, probably because of the high variability observed in this preparation.

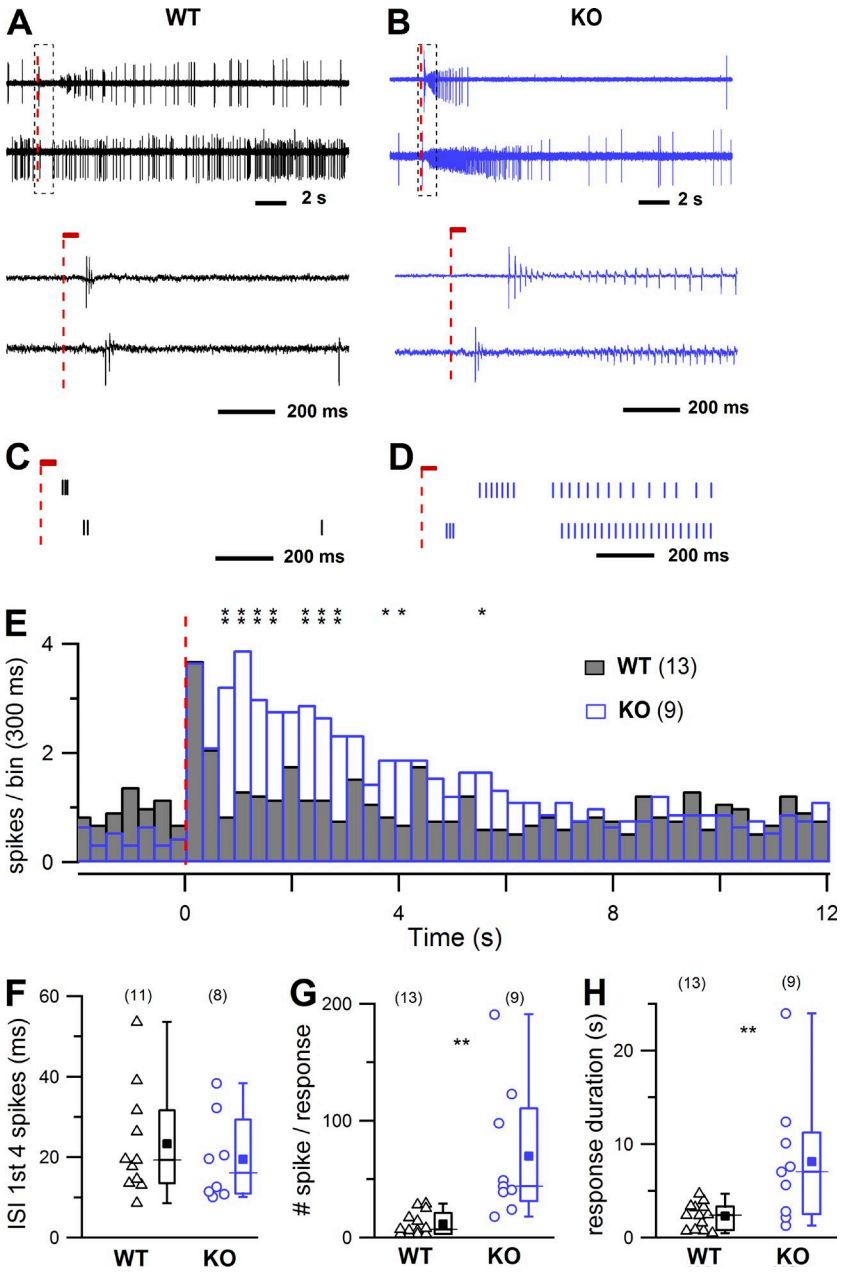

Figure 6. **Evoked activity in OSNs in I7-GFP WT and KO mice for TMEM16B.** (A and B) Representative recordings of responses to a puff of 50 ms of 500 µM heptanal for two different OSNs from WT (A) and KO mice (B). The bottom panels show the regions enclosed by the dashed boxes on an expanded time scale. Broken red lines represent the onset of heptanal stimulation, and the red bars in the bottom panels its duration. (C and D) Raster plots on an enlarged time scale for the same cells shown in A and B. (E) Averaged responses to the same odorant puff as A and B, normalized to the number of neurons (n = 13 from 7 WT mice, n = 9 from 5 KO mice; bin 300 ms). The broken red line represents the onset of stimulation, and data belong to WT and KO PSTH distributions. *, 0.01 < P < 0.05; and **, P < 0.01. (F–H) Scatter plot of ISI of the first four spikes (F; 23 ± 13 ms in WT, 20 ± 11 ms in KO; mean ± SD; Mann-Whitney U test, one tail: P > 0.05), of the total number of spikes (G; 12 ± 10 spike/response in WT, 70 ± 57 spike/response in KO; Mann-Whitney U test, one tail: **, P < 0.01), and of the response duration (H; 2.3 ± 1.3 s in WT, 8.1 ± 7.0 s in KO; Mann-Whitney U test, one tail: **, P < 0.01). In the box plots the squares represent the mean, lines represent the median, upper and lower box boundaries represent the 25th and 75th percentile, and upper and lower whiskers represent the 5th and 95th percentiles. The number of experiments is indicated in parentheses.

Altogether, our results show that both isolated and in situ OSNs from TMEM16B KO mice are able to fire APs in response to a stimulus, although displayed an altered evoked firing pattern. In particular, isolated OSNs from KO mice responded to IBMX with an increased number of APs and a spike train that lasted longer compared with WT OSNs. The spike train distribution recorded from OSNs in situ differed between KO and WT mice, with a higher firing activity of the former group.

Heptanal-induced firing in I7 OSNs

The effectiveness of the IBMX stimulus has large variations among OSNs expressing different ORs (Reisert, 2010), potentially masking differences among evoked activity in OSNs from WT and KO mice. Therefore, we analyzed in detail the odorant-induced firing activity of OSNs that express the I7 OR by crossing I7-IRES-tauGFP (Bozza et al., 2002) with TMEM16B KO mice. Because the mouse I7 gene is expressed mostly in the ventrolateral zone of the olfactory epithelium, we increased the probability of recording from an I7 OSN using a coronal slice preparation from P0–P4 mice, which includes the epithelium attached to the turbinates where I7 OSNs are highly present. Responses to the I7 ligand heptanal (Zhao et al., 1998; Bozza et al., 2002) were recorded from the dendritic knobs of OSNs with the loose-patch configuration. The stimulation consisted of a 50-ms puff of 500 µM heptanal, a stimulus evoking a robust response in I7 OSNs. Fig. 6 (A and B) shows the responses of two representative OSNs for each WT and

KO mice. In the WT, responses to heptanal were similar to those recorded with IBMX (Fig. 5, A and B), i.e., characterized by a short burst of spikes of reducing amplitude, a period of silence, and a rebound of spikes of increasing amplitude (Fig. 6, A and B), as previously described (Tan et al., 2010; Connelly et al., 2013). However, KO OSNs showed longer rebound periods, which added to the overall duration of the response (see Materials and methods) compared with WT OSNs (Fig. 6, A–D). A quantitative characterization of the heptanal responses showed that ISI of the first four spikes did not significantly differ in WT and KO mice (Fig. 6 F), whereas the overall number of spikes and response durations were significantly different (12 ± 10, spike/response and 2.3 ± 1.3 s for WT, and 70 ± 57 spike/response and 8.1 ± 7 s for KO, mean ± SD, Mann-Whitney *U* test, one tail, $P < 0.01$). Thus, I7 OSNs from KO mice showed a prolonged response to heptanal stimulation with a higher number of spikes in the response compared with I7 OSNs from WT mice. The difference between WT and KO I7 OSNs is also highlighted by the cumulative response normalized to the number of neurons (PSTH, Fig. 6 E): the initial peak of activity is followed by a broader one of similar amplitude that is reflecting a prolonged and more intense firing activity in KO with respect to WT I7 OSNs (as quantified in Fig. 6, G and H). The asterisks in the Fig. 6 E represent bins with significantly higher firing rates in KO with respect to WT OSNs (analysis according to Dörrscheidt [1981]). It is worth noting that a similar effect, with an initial peak of activity followed by a broader one, although smaller in amplitude, has been described in Fig. 5 E for IBMX-evoked responses from in situ OSNs.

In summary, by taking advantage of recordings from OSNs expressing the I7 OR, we showed that the lack of CaCCs altered the firing behavior in response to heptanal by increasing the number of spikes and prolonging the duration of the response in isolated OSNs from TMEM16B KO with respect to WT.

Spontaneous firing activity in OSNs

Different OSNs have different levels of basal firing activity, depending on the spontaneous activation of the expressed OR that is driving basal transduction activity (Reisert, 2010; Connelly et al., 2013). Because CaCCs contribute to basal transduction currents as previously demonstrated using the Cl^- channel blocker NFA (Reisert, 2010), we investigated whether the lack of TMEM16B has an effect on the spontaneous spiking activity of OSNs. Spontaneous activity was recorded with on-cell loose-patch recordings from dendritic knobs of OSNs in the intact olfactory epithelium. OSNs showed a wide range of spontaneous firing rates as illustrated by representative recordings of three different WT and KO OSNs and by the corresponding raster plots (Fig. 7, A and B). In WT mice, the pattern of OSNs' spike activ-

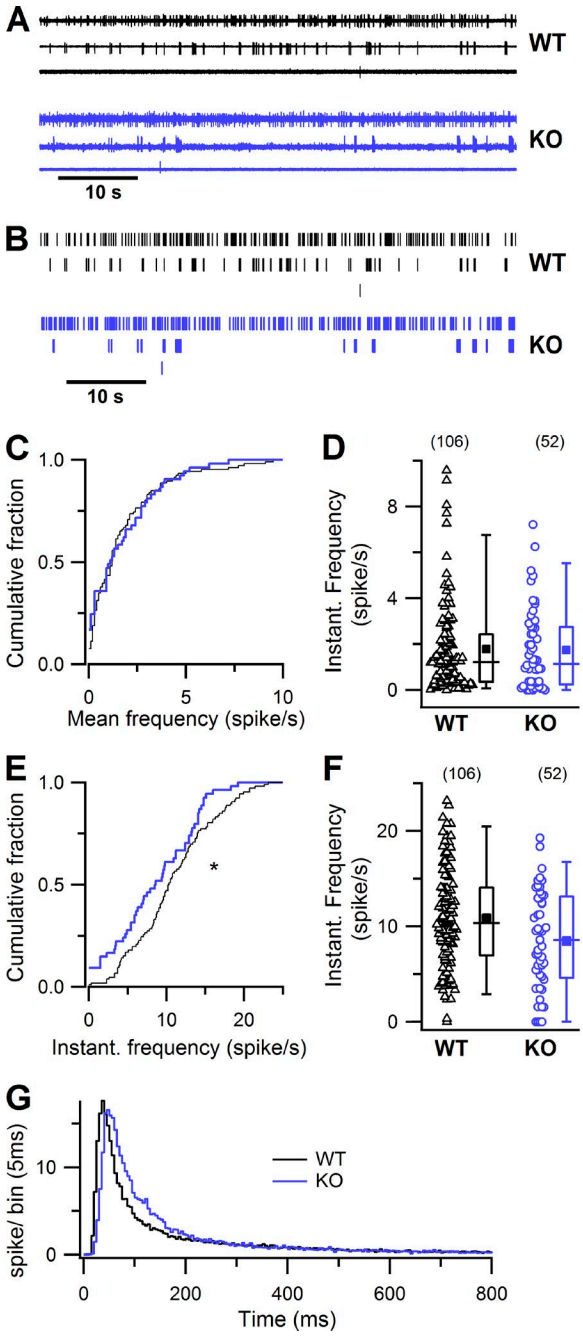

Figure 7. **Spontaneous activity in OSNs in WT and KO mice.** (A and B) Loose-patch recordings (A; 60-s recordings) and raster plots (B) of the spontaneous activity in three WT OSNs (top) and three KO OSNs (bottom). (C and E) Cumulative plot of spontaneous mean (C) and instantaneous (E) firing frequency, bin of 0.1 Hz, in control (black lines) and TMEM16B KO mice (blue lines). Mann-Whitney *U* test, one-tail: $P > 0.05$ for C; *, $0.01 < P < 0.05$ for E. (D and F) Box and scatter plots of spontaneous mean (D) and instantaneous (F) firing activity in OSNs in WT and KO mice. In the box plots, the inner squares represents the mean, lines represent the median, upper and lower box boundaries represent the 25th and 75th percentile, and upper and lower whiskers represent the 5th and 95th percentiles. (G) ISI distribution histogram (bin = 5 ms) normalized to the number of recorded neurons in WT (black line, $n = 106$ from 47 mice) and KO mice (blue line, $n = 52$ from 22 mice).

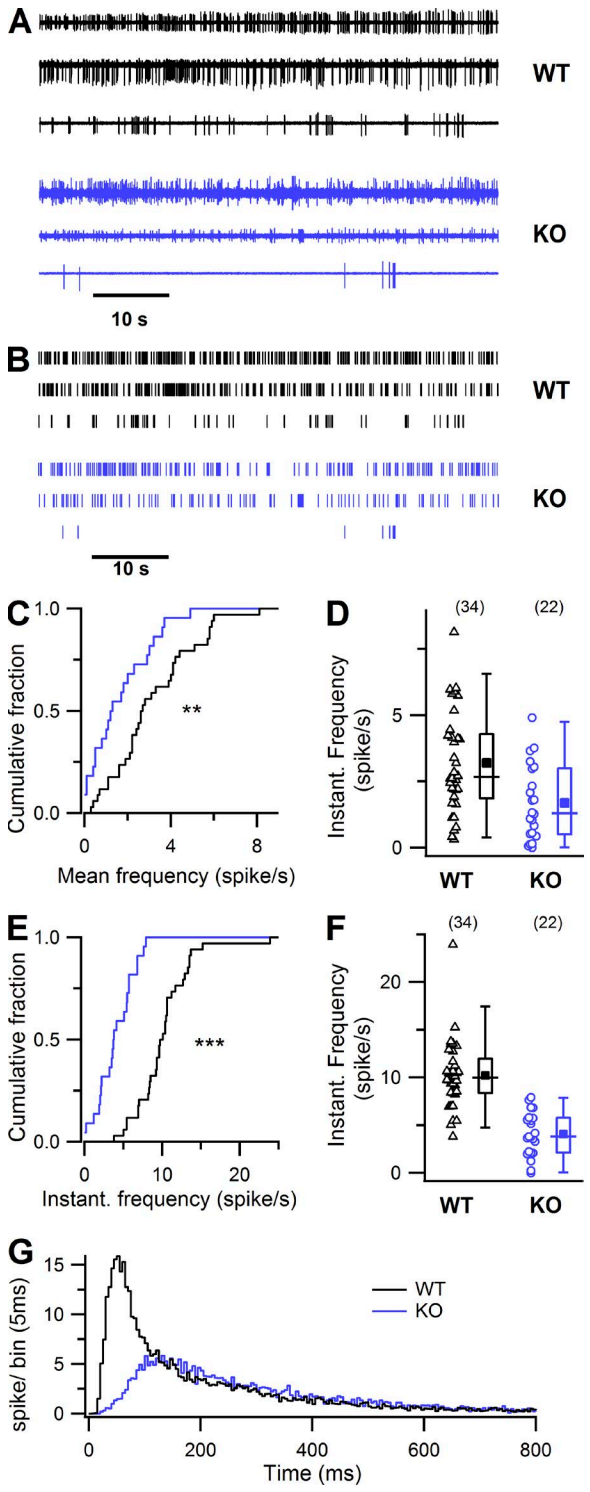

Figure 8. **Spontaneous activity in OSNs from I7-GFP WT and KO mice for TMEM16B.** (A and B) Loose-patch recordings (A; 60-s recordings) and raster plots (B) of the spontaneous firing activity from three WT OSNs (top) and three KO mice (bottom). (C and E) Cumulative plot of spontaneous mean (C) and instantaneous (E) firing frequency, bin of 0.1 Hz, in control (black lines) and TMEM16B KO mice (blue lines). Mann-Whitney *U* test, one-tail: **, $P < 0.01$ in C; and ***, $P < 0.001$ in E. (D and F) Box and scatter plots of spontaneous mean (D) and instantaneous (F) firing activity in OSNs in WT and KO mice. In the box plots, the inner squares represent the mean, lines represent the median, upper and lower box boundaries represent the 25th and 75th percentile, and upper and lower whiskers represent the 5th and 95th percentiles. (G) ISI distribution histogram (bin = 5 ms) normalized to the number of recorded neurons in control (black line, $n = 34$ from 19 mice) and KO mice (blue line, $n = 22$ from 9 mice).

ity was highly variable and confirmed previous studies (Reisert, 2010; Connelly et al., 2013; Lorenzon et al., 2015). A comparison among OSNs from WT and KO mice showed that the mean firing frequency for each neuron, calculated over 2–5-min recording, ranged from 0.0087 to 9.582 in WT and from 0 to 7.22 spikes/s in KO, with mean values of 1.79 ± 1.98 and 1.93 ± 1.93 spikes/s, respectively (mean ± SD; Fig. 7 D). The cumulative distribution of firing frequencies did not reveal any difference between WT and KO OSNs (Fig. 7 C; Mann-Whitney *U* test, one tail, not statistically different). To further investigate the pattern of firing activity, we analyzed the instantaneous firing frequency, calculated as the inverse of the ISI between consecutive spikes. The mean instantaneous firing frequencies were 10.85 ± 5.28 and 8.57 ± 5.22 spikes/s (mean ± SD), respectively, in WT and KO mice (Fig. 7 F). The cumulative distribution showed a shift of the instantaneous firing frequency to lower frequencies for KO compared with WT OSNs (Fig. 7 E; statistically significant, Mann-Whitney *U* test, one tail, $P = 0.0102$). Fig. 7 G shows the distribution of ISIs normalized to the number of recorded neurons. The peak of the KO distribution was slightly shifted to the right compared with WT, reflecting the lower IF for KO compared with WT. Despite the observed variability in spontaneous firing pattern, we found an indication that instantaneous firing frequencies may be reduced in KO OSNs. The large variability most likely originated from the fact that we recorded from randomly picked OSNs expressing a wide variety of ORs with different basal activities, as better shown in experiments obtained from the identified I7 OR (Fig. 8).

Spontaneous firing activity of I7 OSNs decreases in TMEM16B KO mice

To restrict OSN variability, we analyzed spontaneous firing activity of OSNs that express the I7 OR, crossing I7-IRES-tauGFP (Bozza et al., 2002) with TMEM16B KO mice (same mice used for heptanal-induced responses in Fig. 6). Spontaneous activity was recorded with on-cell loose-patch recordings from dendritic knobs of OSNs in coronal slices from P0–P4 mice. Although expressing the same I7 OR, these OSNs also showed some variability in spike activity, as shown by three different WT OSNs in Fig. 8 A, and in agreement with previous studies (Reisert, 2010; Connelly et al., 2013). The mean firing activity of OSNs was significantly lower in KO compared with WT mice (Mann-Whitney *U* test, one tail, $P < 0.01$), as shown

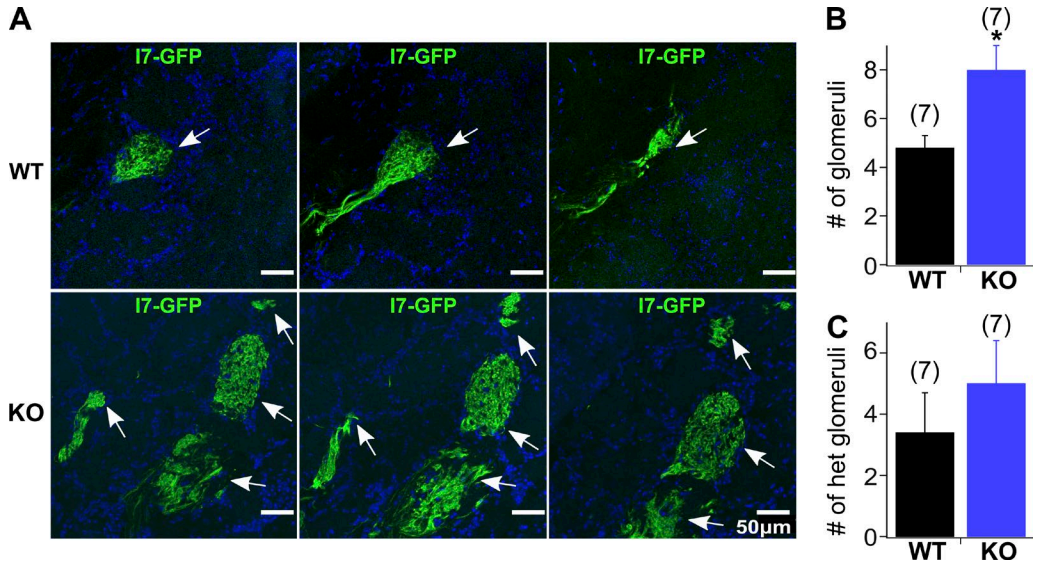

Figure 9. **The number of I7-GFP glomeruli increased in TMEM16B KO mice.** (A) The top row shows a series of three consecutive sagittal sections, where a single I7-GFP glomerulus (pointed by the arrows) is present in a WT mouse. The bottom row shows a series of consecutive sections from a KO mouse, where several glomeruli were observed (arrows). (B) Bar plot representing the total number of glomeruli per animal that significantly increased in the KO (8 ± 1, seven mice) compared with WT (4.8 ± 0.5, seven mice); unpaired *t* test: *, P = 0.015. (C) Bar plot representing the number of heterogeneous glomeruli in WT (black bar, 3.4 ± 3, seven mice) and in KO mice (blue bar, 5 ± 1.4, seven mice). Data are shown as mean ± SEM.

by the cumulative distributions (Fig. 8 C) and by the scatter plot (Fig. 8 D; mean value ± SD, WT 3.19 ± 1.90 spikes/s, KO 1.68 ± 1.40 spikes/s). Additionally, the IF showed a significant reduction in KO compared with WT OSNs (Fig. 8, E and F; mean value ± SD, WT 10.2 ± 3.64 spikes/s, KO 4.05 ± 2.28 spikes/s, Mann-Whitney *U* test, one tail, P < 0.001). The plot of the distribution of ISIs normalized to the number of recorded neurons reveals that brief ISIs were missing in TMEM16B KO neurons compared with WT and that their distribution was shifted to longer ISIs (Fig. 8 G).

The above data clearly show that, despite the high variability, the spontaneous firing is significantly reduced in I7 OR–expressing neurons lacking TMEM16B.

Axonal convergence of I7 OSNs is modified in TMEM16B KO mice

Our electrophysiological data show a reduced spontaneous activity in I7-expressing OSNs in TMEM16B KO compared with WT mice. It is well known that spontaneous OSN spiking activity is required for correct targeting of OSN axons to their glomeruli in the OB and for the establishment and maintenance of the olfactory sensory map (Lodovichi and Belluscio, 2012). For example, recent publications showed that overexpression of the inward rectifying potassium channel (Kir2.1) in OSNs diminishes the excitability of OSNs and indeed severely disrupts the formation of the glomerular map (Yu et al., 2004; Lorenzon et al., 2015).

To investigate whether the altered spiking behavior in I7 OSNs from TMEM16B KO mice affects the fidelity of axonal targeting, we analyzed axonal innervation into glomeruli in the OB by comparing results from sagittal sections of WT and TMEM16B KO OBs. Fig. 9 A shows images of consecutive sagittal sections of a single I7 glomerulus from a WT I7-IRES-tauGFP mouse (Fig. 9 A, top row) and multiple glomeruli in an I7-IRES-tauGFP TMEM16B KO mouse (Fig. 9 A, bottom row). In WT mice, typically one single I7 glomerulus was observed for each side of the OB, whereas in TMEM16B KO mice multiple I7 glomeruli were observed in consecutive sagittal sections (see Fig. 9 A, where up to five glomeruli are visible). In WT, we identified a mean of four I7 glomeruli per mouse in the ventral side of the OB (one lateral and one medial per bulb, Fig. 9 B). In KO mice, the mean number of I7 glomeruli almost doubled compared with WT (Fig. 9 B). The supernumerary glomeruli in TMEM16B KO were evenly scattered in the ventral area of both lateral and medial locations. In addition, some I7 OSN axons innervated additional glomeruli (heterogeneous glomeruli) with a trend toward more glomeruli in TMEM16B KO compared with WT mice, even though this difference did not reach statistical significance (Fig. 9 C).

In conclusion, our results show that TMEM16B contributes to the glomerular formation and refinement of I7-expressing OSNs in the OB.

DISCUSSION

The involvement of CaCCs in odor transduction has been described in the early nineties (Kleene and

Gesteland, 1991; Kleene, 1993, 1997; Kurahashi and Yau, 1993; Lowe and Gold, 1993). In rodents, CaCCs constitute up to 90% (Lowe and Gold, 1993; Boccaccio and Menini, 2007) of the transduction current and Cl^- channels may be eight times more numerous than CNG channels in olfactory cilia (Reisert et al., 2003). The cooperative nature of the current activation by Ca^{2+} significantly contributes to set the dynamic range of OSNs (Lowe and Gold, 1993; Boccaccio et al., 2006). Despite its proposed importance to OSN physiology, the molecular identity of the Ca^{2+}-activated Cl^- channel has been identified as TMEM16B/Anoctamin2 channel only in 2009 (Pifferi et al., 2009; Stephan et al., 2009; Sagheddu et al., 2010). A loss of function approach unequivocally demonstrated that indeed the olfactory Cl^- channel was TMEM16B, but intriguingly it was reported to be dispensable for near-normal olfactory function (Billig et al., 2011). This raises the question of what the purpose of such densely expressed TMEM16B channels in the cilia of OSNs might be.

Odor-guided food-finding ability

An essential behavior for animal survival is the capability to find food, and olfaction plays a very important role in food location. We addressed a possible olfactory-driven behavioral deficit in TMEM16B KO mice by using an odor-guided food-seeking test, which has been largely used to test olfactory acuity in mice (Stephan et al., 2012; Li et al., 2013). The test does not rely on any specific mouse training, e.g., learning of an operant-conditioning task, but instead mice have to rely on their naive sense of smell to locate the odor source of food. When confronted with novel odors, TMEM16B KO required longer times to locate the food compared with WT mice, whereas for odors already known to the mice, e.g., retesting with the same food, they performed equally well. KO mice required longer times to find novel foods even when they performed equally well on known odors, suggesting that the observed difference between WT and KO is not a simple lack of motivation, deficit in locomotion, or inability to perform the task. It is tempting to speculate that the observed glomerular mistargeting and/or altered AP firing in TMEM16B KO mice may be the underlying causes for the observed olfactory-driven behavioral deficit, an issue that future experiments will have to address. Particularly interesting may be the apparent conundrum between the decreased ability to recognize new odors and increased firing. It is worth noticing that an increase in AP firing does not necessarily mean a better olfactory coding capability because it may result in a failure to synchronize the breathing cycle with the sniffing cycle (Ghatpande and Reisert, 2011; Dibattista and Reisert, 2016). Billig et al. (2011) did not observe behavioral deficits in an odor-guided operant conditioning task in apparent contradiction to our findings here. This difference might originate in the different behavioral test used. Operant conditioning requires extensive training, repeated exposure to an odor, and often averaging over many trials. Given that TMEM16B KO mice only showed deficits on the first few exposures to new odors, such a behavioral deficit might be difficult to investigate using such an approach. Another interesting difference is the odor source used in the two approaches.

The operant conditioning task required the mouse to smell monomolecular odorants, whereas in our task mice were challenged to smell a complex mixture of multiple odorants, which has been shown to activate a denser glomerular response (Vincis et al., 2012). Moreover, it has been recently shown that the hedonic value of an odor object is topographically encoded along the anteroposterior axis of the ventral side of OB (Kermen et al., 2016), adding further evidence to the idea odor recognition requires a well-organized glomerular map (Kobayakawa et al., 2007; Dewan et al., 2013), where perturbations, e.g., an increase in targeted glomeruli as we report, can prove detrimental.

TMEM16B channel is responsible for the generation of CaCCs in OSN cilia and controls evoked firing in OSNs

In agreement with a previous study (Billig et al., 2011), we confirmed here that CaCCs were absent in isolated OSNs from TMEM16B KO mice (Figs. 2 and 3), further supporting the notion that the CaCC is the major contributor to the transduction current in isolated OSNs. Moreover, we showed that NFA, a blocker of the CaCC, did not further block the remaining ciliary current in KO OSNs using the suction electrode technique. Indeed, as with the suction electrode technique only the cilia and dendritic knob of an OSN are exposed to the solution exchange (and hence to the blocker), we could exclude that NFA might have had unspecific effects on other channels expressed in the dendrite or soma of OSNs. Thus, we confirm that TMEM16B is responsible for CaCCs in OSN cilia.

Importantly, AP firing along OSN axons transfers information about odors to the OB. Here, we first investigated the ability of TMEM16B KO OSNs to generate APs in response to a stimulus, an aspect that was not addressed in the previous paper by Billig et al. (2011) and that we measured with various recording methods and configurations. After establishing that the resting membrane potential and the input resistance are not significantly different in OSNs from TMEM16B WT and KO mice, we compared AP firing in OSNs from WT and KO mice using suction electrode recordings from isolated OSNs (Fig. 4). Despite the strong reduction of the transduction current in isolated TMEM16B KO OSNs, on average, we measured longer trains and a higher number of APs in response to the phosphodiesterase

inhibitor IBMX compared with WT OSNs (Fig. 4), suggesting that TMEM16B contributes to shorten IBMX-evoked firing activity.

We also extended our experiments to OSNs recorded in situ (Fig. 5) in the intact olfactory epithelium, a situation more closely resembling the physiological OSN conditions. The cumulative distribution of the evoked responses indicated an increase in firing activity in KO with respect to WT mice (IBMX in Fig. 5 E and heptanal in Fig. 6 E). The contribution of CaCC was more evident in the heptanal responses of OSNs expressing the I7 OR, probably because of lower intrinsic variability, as in this case we recorded from a defined set of OSNs expressing one known OR.

How does TMEM16B regulate firing duration and number of spikes? APs are generated during the rising phase of the receptor current and display a progressive loss of amplitude during the spike train down to zero levels at which APs firing is absent (Reisert and Matthews, 2001; Savigner et al., 2009), leading to a shortening of the spike train. This spike disappearance originates from progressive inactivation of voltage-gated Na^+ and Ca^{2+} channels during prolonged and strong depolarization (Trotier, 1994). The lack of a substantial transduction current, as observed in isolated TMEM16B KO OSNs (Fig. 3), likely affects the depolarization of OSNs, causing a reduced or slower inactivation of voltage-gated channels, allowing for more spikes to be generated over a longer time window. Thus, although the presence of CNG currents is necessary and sufficient to generate APs in response to a stimulus, CaCCs contribute to regulating firing duration and number of spikes.

TMEM16B increases the spontaneous firing rate in OSNs

It is well established that spontaneous activity in OSNs significantly contributes to the development and physiology of the olfactory system (Nakashima et al., 2013b; Lorenzon et al., 2015). Moreover, different ORs have various basal activities (Reisert, 2010), which stimulate the signal transduction cascade to drive basal cAMP fluctuations, opening of CNG channels followed by TMEM16B channels, and AP generation. Here, the availability of TMEM16B KO mice gave us the possibility to directly investigate how the absence of CaCCs affects the spontaneous activity in OSNs. On average, OSNs expressing random ORs showed a mild decrease in the instantaneous firing frequency in TMEM16B KO compared with WT mice (Fig. 7 E). Interestingly, OSNs expressing the I7 OR, a receptor known to have a relatively high spontaneous activity (as shown by Reisert [2010] in dissociated OSNs and by Connelly et al. [2013] from in situ OSNs in the intact olfactory epithelia), showed a strong reduction of both instantaneous and mean firing frequencies in the absence of TMEM16B (Fig. 8, C and E). Thus, CaCCs contribute to the spontaneous firing activity of I7 OSNs by amplifying the current through CNG channels, which itself is driven by baseline cAMP fluctuations. It is likely that OSNs expressing ORs with a basal activity lower than that of I7 would not be affected by the lack of TMEM16B as much as the I7 OR. Indeed, OSNs expressing random ORs did not show a reduced mean firing activity (Fig. 7 C), but only a decrease in the instantaneous firing frequency (Fig. 7 E).

The mean and instantaneous firing frequencies we recorded from I7-expressing OSNs from newborn mice strongly resembled the values obtained from adult mice shown in Fig. 1 (B and D) of Connelly et al. (2013). Although our recordings from neurons expressing a random OR are obtained from adult animals, the above observation makes it unlikely that the difference observed is caused by animals' age rather than by the expressed OR.

Thus, the small activation of CaCCs likely occurring in basal conditions contributes to neurons' depolarization and supports spontaneous spike generation.

Proper glomerular formation in the OB requires the presence of TMEM16B

Axons from OSNs expressing the same OR coalesce together in the OB where they typically form one laterally and one medially located glomerulus in each bulb. The process of glomerular formation and refinement is highly dependent by the OR type an OSN expresses (Nakashima et al., 2013b; Nishizumi and Sakano, 2015). On top of activity-independent mechanisms, neuronal activity is important for circuitry formation in visual and auditory systems (Huberman et al., 2008; Wang et al., 2015) as well as in the olfactory system (Yu et al., 2004; Lodovichi and Belluscio, 2012; Nakashima et al., 2013b; Lorenzon et al., 2015), where it is involved in segregation of axons into glomerular structures (see Nishizumi and Sakano [2015] for review).

Hitherto glomerular targeting in TMEM16B KO mice has been investigated for the P2 and M72 ORs (Billig et al., 2011), and no apparent lack of axonal coalescence into glomeruli was observed, whereas the number of innervated glomeruli in WT and KO animals remained unclear. Here, we investigated axonal targeting for the I7 OR and demonstrated that nearly twice as many glomeruli were formed in TMEM16B KO compared with WT mice (Fig. 9). This indicates that TMEM16B plays a relevant role for glomerular targeting of OSNs expressing the I7 OR. Furthermore, TMEM16B may be necessary for proper glomerular targeting of some, but not all ORs, possibly by regulating basal and/or odorant-induced activity. This is consistent with previous observations where in the same genetically modified animal models different ORs showed different glomerular targeting or mistargeting phenotypes (Zheng et al., 2000; Yu et al., 2004; Mobley et al., 2010; Lorenzon et al., 2015). In-

terestingly, OSNs of Kir2.1 knock-in mice have a reduced spontaneous firing activity compared with WT and also show some supernumerary glomeruli (Lorenzon et al., 2015), similarly to what we observed in TMEM16B KO mice.

By combining different recording methods and configurations, we found that the Ca^{2+}-activated Cl^- channel TMEM16B modulates olfactory function in unexpected ways by reducing and shortening stimulus-induced firing, but increasing spontaneous firing activity. The extent by which CaCCs affect firing may depend on the OR that an OSN expresses. Also, experiments on I7 expressing OSNs were performed in P0–P4 mice, and one might argue that these neurons do not represent an OSN in an adult animal. But even at this young age, all the elements of signal transduction cascade are in place (Maurya and Menini, 2014), and OSNs are considered mature OSNs based on their OMP expression. In addition, it seems that there is not a clear difference in odorant sensitivity between OSNs at different ages (Lam and Mombaerts, 2013), and NFA, a blocker of CaCCs, suppresses basal activity in I7-expressing OSNs obtained from adult mice (Reisert, 2010), mirroring the reduced basal activity we observed here in TMEM16B KO OSNs.

Thus, TMEM16B would have a dual role in the control of firing activity in OSN. Indeed, although random activation of TMEM16B Cl^- channels in the cilia, caused by spontaneous small cAMP fluctuations, facilitates small depolarizations that lead to AP generation at a low frequency, strong activation, after odorant stimulation, likely induces a strong depolarization that appears to inhibit spiking, most likely because of Na^+ channel inactivation during prolonged depolarization. In the absence of TMEM16B, the total depolarization would be likely smaller, reducing Na^+ channel inactivation. Further experiments will be necessary to investigate these hypotheses.

Additionally, TMEM16B ensures correct glomerular targeting of I7 receptor–expressing OSNs. In TMEM16B KO mice, the impaired ability of forming a proper glomerular map along with the altered AP firing in response to odorants may contribute to the olfactory-driven impairment in food-finding behavior that we observed, thus making the CaCCs relevant for the OSN physiology and for the functioning of the olfactory system as a whole.

From single-cell physiology to behavior

A striking finding of our work is that OSNs in the absence of TMEM16B altered their firing in response to a stimulus. In particular, the spike number and spike train duration increased in TMEM16B KO OSNs, thus indicating that CaCCs are important in controlling AP firing. In OSNs, odorant concentration could be encoded by the number of spikes generated and the spike train duration (Reisert and Matthews, 1999; Rospars et al., 2003), which our results showed to be controlled by TMEM16B. An altered number of spikes after odorant stimulation may alter the optimal dynamic range of an OSN, thus resulting in a disruption of the glomerular map activation beyond the increased number of targeted glomeruli we observed because it has been reported that increasing odorant concentration increases glomerular recruitment (Wachowiak and Cohen, 2001; Bozza et al., 2004; Vincis et al., 2012). Different odorant concentrations that are represented in the activation of the glomerular map could be perceived with different intensity (reviewed by Mainland et al., 2014). In addition, because the glomerular projections of ORs (most likely preferentially those with higher spontaneous activity) are controlled by TMEM16B, a large change in spatial map could potentially confuse odor intensity and quality codes, as it happened in our case when TMEM16B mice could not perform the behavioral task as efficiently as the WT. Also, an increased spike train duration will make it more difficult for OSN firing to stay entrained to the breathing and sniffing frequency with which a mouse samples its environment, leading to potential ambiguity over which sniff cycle elicited which spike train.

ACKNOWLEDGMENTS

We thank Dr. Thomas Jentsch, Dr. Gwendolyn Billig, and Jonas Münch for providing TMEM16B KO mice and Dr. Peter Mombaerts for providing I7-IRES-tauGFP mice. We also thank Dr. Thomas Jentsch and Dr. Graeme Lowe for insightful discussions and comments to the manuscript, Dr. Xavier Grosmaitre for valuable suggestions on perforated patch, and Dr. Joachim Scholz-Starke and all members of the laboratories for discussions. We thank John Lees for expert assistance with mouse behavioral experiments. Immunohistochemistry and confocal microscopy was performed at the Monell Histology and Cellular Localization Core. Genotyping was performed at SISSA by Jessica Franzot or at the Monell Genotyping and DNA/RNA Analysis Core, which are supported, in part, by funding from the National Institutes of Health (NIH)–National Institute on Deafness and Other Communication Disorders Core Grant 1P30DC011735-01.

This study was supported by grants from the Italian Ministry of Education, University, and Research (2010599KBR to A. Menini), from the Fondazione Compagnia di San Paolo, Torino (2013.0922 to A. Boccaccio), and from the NIH (DC009613 to J. Reisert) and also from infrastructure improvement at the Monell Chemical Senses Center (grant G20OD020296).

The authors declare no competing financial interests.

Author contributions: M. Dibattista performed behavioral experiments. G. Pietra and M. Dibattista performed whole epithelium and single-cell electrophysiological experiments, respectively, and conducted immunohistological experiments. A. Boccaccio performed uncaging patch-clamp experiments. G. Pietra, M. Dibattista, A. Menini, J. Reisert, and A. Boccaccio conceptualized and analyzed experiments and wrote the manuscript.

Richard W. Aldrich served as editor.

Submitted: 16 May 2016
Accepted: 8 August 2016

REFERENCES

Billig, G.M., B. Pál, P. Fidzinski, and T.J. Jentsch. 2011. Ca^{2+}-activated Cl^- currents are dispensable for olfaction. *Nat. Neurosci.* 14:763–769. http://dx.doi.org/10.1038/nn.2821

Boccaccio, A., and A. Menini. 2007. Temporal development of cyclic nucleotide-gated and Ca^{2+}-activated Cl^- currents in isolated mouse olfactory sensory neurons. *J. Neurophysiol.* 98:153–160. http://dx.doi.org/10.1152/jn.00270.2007

Boccaccio, A., L. Lagostena, V. Hagen, and A. Menini. 2006. Fast adaptation in mouse olfactory sensory neurons does not require the activity of phosphodiesterase. *J. Gen. Physiol.* 128:171–184. http://dx.doi.org/10.1085/jgp.200609555

Boccaccio, A., C. Sagheddu, and A. Menini. 2011. Flash photolysis of caged compounds in the cilia of olfactory sensory neurons. *J. Vis. Exp.* (55):e3195.

Bozza, T., P. Feinstein, C. Zheng, and P. Mombaerts. 2002. Odorant receptor expression defines functional units in the mouse olfactory system. *J. Neurosci.* 22:3033–3043.

Bozza, T., J.P. McGann, P. Mombaerts, and M. Wachowiak. 2004. In vivo imaging of neuronal activity by targeted expression of a genetically encoded probe in the mouse. *Neuron.* 42:9–21. http://dx.doi.org/10.1016/S0896-6273(04)00144-8

Connelly, T., A. Savigner, and M. Ma. 2013. Spontaneous and sensory-evoked activity in mouse olfactory sensory neurons with defined odorant receptors. *J. Neurophysiol.* 110:55–62. http://dx.doi.org/10.1152/jn.00910.2012

Delay, R., and D. Restrepo. 2004. Odorant responses of dual polarity are mediated by cAMP in mouse olfactory sensory neurons. *J. Neurophysiol.* 92:1312–1319. http://dx.doi.org/10.1152/jn.00140.2004

Dewan, A., R. Pacifico, R. Zhan, D. Rinberg, and T. Bozza. 2013. Non-redundant coding of aversive odours in the main olfactory pathway. *Nature.* 497:486–489. http://dx.doi.org/10.1038/nature12114

Dibattista, M., and J. Reisert. 2016. The odorant receptor-dependent role of olfactory marker protein in olfactory receptor neurons. *J. Neurosci.* 36:2995–3006. http://dx.doi.org/10.1523/JNEUROSCI.4209-15.2016

Dörrscheidt, G.H. 1981. The statistical significance of the peristimulus time histogram (PSTH). *Brain Res.* 220:397–401. http://dx.doi.org/10.1016/0006-8993(81)91232-4

Duchamp-Viret, P., A. Duchamp, and M.A. Chaput. 2000. Peripheral odor coding in the rat and frog: quality and intensity specification. *J. Neurosci.* 20:2383–2390.

Firestein, S., and G.M. Shepherd. 1995. Interaction of anionic and cationic currents leads to a voltage dependence in the odor response of olfactory receptor neurons. *J. Neurophysiol.* 73:562–567.

Frings, S., and B. Lindemann. 1991. Current recording from sensory cilia of olfactory receptor cells in situ. I. The neuronal response to cyclic nucleotides. *J. Gen. Physiol.* 97:1–16. http://dx.doi.org/10.1085/jgp.97.1.1

Ghatpande, A.S., and J. Reisert. 2011. Olfactory receptor neuron responses coding for rapid odour sampling. *J. Physiol.* 589:2261–2273. http://dx.doi.org/10.1113/jphysiol.2010.203687

Grosmaitre, X., L.C. Santarelli, J. Tan, M. Luo, and M. Ma. 2007. Dual functions of mammalian olfactory sensory neurons as odor detectors and mechanical sensors. *Nat. Neurosci.* 10:348–354. http://dx.doi.org/10.1038/nn1856

Hall, S.E., W.B. Floriano, N. Vaidehi, and W.A. Goddard III. 2004. Predicted 3-D structures for mouse I7 and rat I7 olfactory receptors and comparison of predicted odor recognition profiles with experiment. *Chem. Senses.* 29:595–616. http://dx.doi.org/10.1093/chemse/bjh063

Huberman, A.D., M.B. Feller, and B. Chapman. 2008. Mechanisms underlying development of visual maps and receptive fields. *Annu. Rev. Neurosci.* 31:479–509. http://dx.doi.org/10.1146/annurev.neuro.31.060407.125533

Imai, T., M. Suzuki, and H. Sakano. 2006. Odorant receptor-derived cAMP signals direct axonal targeting. *Science.* 314:657–661. http://dx.doi.org/10.1126/science.1131794

Jarriault, D., and X. Grosmaitre. 2015. Perforated patch-clamp recording of mouse olfactory sensory neurons in intact neuroepithelium: functional analysis of neurons expressing an identified odorant receptor. *J. Vis. Exp.* (101):e52652.

Kaneko, H., I. Putzier, S. Frings, U.B. Kaupp, and T. Gensch. 2004. Chloride accumulation in mammalian olfactory sensory neurons. *J. Neurosci.* 24:7931–7938. http://dx.doi.org/10.1523/JNEUROSCI.2115-04.2004

Kermen, F., M. Midroit, N. Kuczewski, J. Forest, M. Thévenet, J. Sacquet, C. Benetollo, M. Richard, A. Didier, and N. Mandairon. 2016. Topographical representation of odor hedonics in the olfactory bulb. *Nat. Neurosci.* 19:876–878. http://dx.doi.org/10.1038/nn.4317

Kleene, S.J. 1993. Origin of the chloride current in olfactory transduction. *Neuron.* 11:123–132. http://dx.doi.org/10.1016/0896-6273(93)90276-W

Kleene, S.J. 1997. High-gain, low-noise amplification in olfactory transduction. *Biophys. J.* 73:1110–1117. http://dx.doi.org/10.1016/S0006-3495(97)78143-8

Kleene, S.J. 2008. The electrochemical basis of odor transduction in vertebrate olfactory cilia. *Chem. Senses.* 33:839–859. http://dx.doi.org/10.1093/chemse/bjn048

Kleene, S.J., and R.C. Gesteland. 1991. Calcium-activated chloride conductance in frog olfactory cilia. *J. Neurosci.* 11:3624–3629.

Kobayakawa, K., R. Kobayakawa, H. Matsumoto, Y. Oka, T. Imai, M. Ikawa, M. Okabe, T. Ikeda, S. Itohara, T. Kikusui, et al. 2007. Innate versus learned odour processing in the mouse olfactory bulb. *Nature.* 450:503–508. http://dx.doi.org/10.1038/nature06281

Krautwurst, D., K.W. Yau, and R.R. Reed. 1998. Identification of ligands for olfactory receptors by functional expression of a receptor library. *Cell.* 95:917–926. http://dx.doi.org/10.1016/S0092-8674(00)81716-X

Kurahashi, T., and K.W. Yau. 1993. Co-existence of cationic and chloride components in odorant-induced current of vertebrate olfactory receptor cells. *Nature.* 363:71–74. http://dx.doi.org/10.1038/363071a0

Lagostena, L., and A. Menini. 2003. Whole-cell recordings and photolysis of caged compounds in olfactory sensory neurons isolated from the mouse. *Chem. Senses.* 28:705–716. http://dx.doi.org/10.1093/chemse/bjg063

Lam, R.S., and P. Mombaerts. 2013. Odorant responsiveness of embryonic mouse olfactory sensory neurons expressing the odorant receptors S1 or MOR23. *Eur. J. Neurosci.* 38:2210–2217. http://dx.doi.org/10.1111/ejn.12240

Li, F., S. Ponissery-Saidu, K.K. Yee, H. Wang, M.-L. Chen, N. Iguchi, G. Zhang, P. Jiang, J. Reisert, and L. Huang. 2013. Heterotrimeric G protein subunit Gγ13 is critical to olfaction. *J. Neurosci.* 33:7975–7984. http://dx.doi.org/10.1523/JNEUROSCI.5563-12.2013

Lodovichi, C., and L. Belluscio. 2012. Odorant receptors in the formation of the olfactory bulb circuitry. *Physiology (Bethesda).* 27:200–212. http://dx.doi.org/10.1152/physiol.00015.2012

Lorenzon, P., N. Redolfi, M.J. Podolsky, I. Zamparo, S.A. Franchi, G. Pietra, A. Boccaccio, A. Menini, V.N. Murthy, and C. Lodovichi. 2015. Circuit formation and function in the olfactory bulb of mice with reduced spontaneous afferent activity. *J. Neurosci.* 35:146–160. http://dx.doi.org/10.1523/JNEUROSCI.0613-14.2015

Lowe, G., and G.H. Gold. 1991. The spatial distributions of odorant sensitivity and odorant-induced currents in salamander olfactory

receptor cells. *J. Physiol.* 442:147–168. http://dx.doi.org/10.1113/jphysiol.1991.sp018787

Lowe, G., and G.H. Gold. 1993. Nonlinear amplification by calcium-dependent chloride channels in olfactory receptor cells. *Nature.* 366:283–286. http://dx.doi.org/10.1038/366283a0

Lowe, G., and G.H. Gold. 1995. Olfactory transduction is intrinsically noisy. *Proc. Natl. Acad. Sci. USA.* 92:7864–7868. http://dx.doi.org/10.1073/pnas.92.17.7864

Ma, M., W.R. Chen, and G.M. Shepherd. 1999. Electrophysiological characterization of rat and mouse olfactory receptor neurons from an intact epithelial preparation. *J. Neurosci. Methods.* 92:31–40. http://dx.doi.org/10.1016/S0165-0270(99)00089-8

Mainland, J.D., J.N. Lundström, J. Reisert, and G. Lowe. 2014. From molecule to mind: an integrative perspective on odor intensity. *Trends Neurosci.* 37:443–454. http://dx.doi.org/10.1016/j.tins.2014.05.005

Matthews, H.R. 1999. A compact modular flow heater for the superfusion of mammalian cells. *J. Physiol.* 518:13P.

Maurya, D.K., and A. Menini. 2014. Developmental expression of the calcium-activated chloride channels TMEM16A and TMEM16B in the mouse olfactory epithelium. *Dev. Neurobiol.* 74:657–675. http://dx.doi.org/10.1002/dneu.22159

Mobley, A.S., A.M. Miller, R.C. Araneda, L.R. Maurer, F. Müller, and C.A. Greer. 2010. Hyperpolarization-activated cyclic nucleotide-gated channels in olfactory sensory neurons regulate axon extension and glomerular formation. *J. Neurosci.* 30:16498–16508. http://dx.doi.org/10.1523/JNEUROSCI.4225-10.2010

Nakamura, T., and G.H. Gold. 1987. A cyclic nucleotide-gated conductance in olfactory receptor cilia. *Nature.* 325:442–444. http://dx.doi.org/10.1038/325442a0

Nakashima, A., H. Takeuchi, T. Imai, H. Saito, H. Kiyonari, T. Abe, M. Chen, L.S. Weinstein, C.R. Yu, D.R. Storm, et al. 2013b. Agonist-independent GPCR activity regulates anterior-posterior targeting of olfactory sensory neurons. *Cell.* 154:1314–1325. http://dx.doi.org/10.1016/j.cell.2013.08.033

Nakashima, N., T.M. Ishii, Y. Bessho, R. Kageyama, and H. Ohmori. 2013a. Hyperpolarisation-activated cyclic nucleotide-gated channels regulate the spontaneous firing rate of olfactory receptor neurons and affect glomerular formation in mice. *J. Physiol.* 591:1749–1769. http://dx.doi.org/10.1113/jphysiol.2012.247361

Nickell, W.T., N.K. Kleene, R.C. Gesteland, and S.J. Kleene. 2006. Neuronal chloride accumulation in olfactory epithelium of mice lacking NKCC1. *J. Neurophysiol.* 95:2003–2006. http://dx.doi.org/10.1152/jn.00962.2005

Nishizumi, H., and H. Sakano. 2015. Developmental regulation of neural map formation in the mouse olfactory system. *Dev. Neurobiol.* 75:594–607. http://dx.doi.org/10.1002/dneu.22268

Nunemaker, C.S., R.A. DeFazio, and S.M. Moenter. 2003. A targeted extracellular approach for recording long-term firing patterns of excitable cells: a practical guide. *Biol. Proced. Online.* 5:53–62. http://dx.doi.org/10.1251/bpo46

O'Connell, R.J., and M.M. Mozell. 1969. Quantitative stimulation of frog olfactory receptors. *J. Neurophysiol.* 32:51–63.

Pedemonte, N., and L.J.V. Galietta. 2014. Structure and function of TMEM16 proteins (anoctamins). *Physiol. Rev.* 94:419–459. http://dx.doi.org/10.1152/physrev.00039.2011

Pifferi, S., A. Boccaccio, and A. Menini. 2006. Cyclic nucleotide-gated ion channels in sensory transduction. *FEBS Lett.* 580:2853–2859. http://dx.doi.org/10.1016/j.febslet.2006.03.086

Pifferi, S., M. Dibattista, and A. Menini. 2009. TMEM16B induces chloride currents activated by calcium in mammalian cells. *Pflugers Arch.* 458:1023–1038. http://dx.doi.org/10.1007/s00424-009-0684-9

Pifferi, S., A. Menini, and T. Kurahashi. 2010. Signal transduction in vertebrate olfactory cilia. In The Neurobiology of Olfaction. Frontiers in Neuroscience. First edition. A. Menini, editor. CRC Press, Boca Raton, FL. 203–224.

Pifferi, S., V. Cenedese, and A. Menini. 2012. Anoctamin 2/TMEM16B: a calcium-activated chloride channel in olfactory transduction. *Exp. Physiol.* 97:193–199. http://dx.doi.org/10.1113/expphysiol.2011.058230

Ponissery Saidu, S., M. Dibattista, H.R. Matthews, and J. Reisert. 2012. Odorant-induced responses recorded from olfactory receptor neurons using the suction pipette technique. *J. Vis. Exp.* (62):e3862.

Reisert, J. 2010. Origin of basal activity in mammalian olfactory receptor neurons. *J. Gen. Physiol.* 136:529–540. http://dx.doi.org/10.1085/jgp.201010528

Reisert, J., and H.R. Matthews. 1999. Adaptation of the odour-induced response in frog olfactory receptor cells. *J. Physiol.* 519:801–813. http://dx.doi.org/10.1111/j.1469-7793.1999.0801n.x

Reisert, J., and H.R. Matthews. 2001. Response properties of isolated mouse olfactory receptor cells. *J. Physiol.* 530:113–122. http://dx.doi.org/10.1111/j.1469-7793.2001.0113m.x

Reisert, J., P.J. Bauer, K.-W. Yau, and S. Frings. 2003. The Ca-activated Cl channel and its control in rat olfactory receptor neurons. *J. Gen. Physiol.* 122:349–364. http://dx.doi.org/10.1085/jgp.200308888

Reisert, J., J. Lai, K.-W. Yau, and J. Bradley. 2005. Mechanism of the excitatory Cl^- response in mouse olfactory receptor neurons. *Neuron.* 45:553–561. http://dx.doi.org/10.1016/j.neuron.2005.01.012

Reisert, J., K.-W. Yau, and F.L. Margolis. 2007. Olfactory marker protein modulates the cAMP kinetics of the odour-induced response in cilia of mouse olfactory receptor neurons. *J. Physiol.* 585:731–740. http://dx.doi.org/10.1113/jphysiol.2007.142471

Reuter, D., K. Zierold, W.H. Schröder, and S. Frings. 1998. A depolarizing chloride current contributes to chemoelectrical transduction in olfactory sensory neurons in situ. *J. Neurosci.* 18:6623–6630.

Rospars, J.-P., P. Lánský, A. Duchamp, and P. Duchamp-Viret. 2003. Relation between stimulus and response in frog olfactory receptor neurons in vivo. *Eur. J. Neurosci.* 18:1135–1154. http://dx.doi.org/10.1046/j.1460-9568.2003.02766.x

Sagheddu, C., A. Boccaccio, M. Dibattista, G. Montani, R. Tirindelli, and A. Menini. 2010. Calcium concentration jumps reveal dynamic ion selectivity of calcium-activated chloride currents in mouse olfactory sensory neurons and TMEM16b-transfected HEK 293T cells. *J. Physiol.* 588:4189–4204. http://dx.doi.org/10.1113/jphysiol.2010.194407

Savigner, A., P. Duchamp-Viret, X. Grosmaitre, M. Chaput, S. Garcia, M. Ma, and B. Palouzier-Paulignan. 2009. Modulation of spontaneous and odorant-evoked activity of rat olfactory sensory neurons by two anorectic peptides, insulin and leptin. *J. Neurophysiol.* 101:2898–2906. http://dx.doi.org/10.1152/jn.91169.2008

Schild, D., and D. Restrepo. 1998. Transduction mechanisms in vertebrate olfactory receptor cells. *Physiol. Rev.* 78:429–466.

Shimazaki, H., and S. Shinomoto. 2007. A method for selecting the bin size of a time histogram. *Neural Comput.* 19:1503–1527. http://dx.doi.org/10.1162/neco.2007.19.6.1503

Stephan, A.B., E.Y. Shum, S. Hirsh, K.D. Cygnar, J. Reisert, and H. Zhao. 2009. ANO2 is the cilial calcium-activated chloride channel that may mediate olfactory amplification. *Proc. Natl. Acad. Sci. USA.* 106:11776–11781. http://dx.doi.org/10.1073/pnas.0903304106

Stephan, A.B., S. Tobochnik, M. Dibattista, C.M. Wall, J. Reisert, and H. Zhao. 2012. The Na^+/Ca^{2+} exchanger NCKX4 governs

termination and adaptation of the mammalian olfactory response. *Nat. Neurosci.* 15:131–137. http://dx.doi.org/10.1038/nn.2943

Tan, J., A. Savigner, M. Ma, and M. Luo. 2010. Odor information processing by the olfactory bulb analyzed in gene-targeted mice. *Neuron.* 65:912–926. http://dx.doi.org/10.1016/j.neuron.2010.02.011

Trotier, D. 1994. Intensity coding in olfactory receptor cells. *Semin. Cell Biol.* 5:47–54. http://dx.doi.org/10.1006/scel.1994.1007

Trotier, D. 1998. Electrophysiological properties of frog olfactory supporting cells. *Chem. Senses.* 23:363–369. http://dx.doi.org/10.1093/chemse/23.3.363

Trotier, D., and P. MacLeod. 1983. Intracellular recordings from salamander olfactory receptor cells. *Brain Res.* 268:225–237. http://dx.doi.org/10.1016/0006-8993(83)90488-2

Vincis, R., O. Gschwend, K. Bhaukaurally, J. Beroud, and A. Carleton. 2012. Dense representation of natural odorants in the mouse olfactory bulb. *Nat. Neurosci.* 15:537–539. http://dx.doi.org/10.1038/nn.3057

Wachowiak, M., and L.B. Cohen. 2001. Representation of odorants by receptor neuron input to the mouse olfactory bulb. *Neuron.* 32:723–735. http://dx.doi.org/10.1016/S0896-6273(01)00506-2

Wang, H.C., C.-C. Lin, R. Cheung, Y. Zhang-Hooks, A. Agarwal, G. Ellis-Davies, J. Rock, and D.E. Bergles. 2015. Spontaneous activity of cochlear hair cells triggered by fluid secretion mechanism in adjacent support cells. *Cell.* 163:1348–1359. http://dx.doi.org/10.1016/j.cell.2015.10.070

Yu, C.R., J. Power, G. Barnea, S. O'Donnell, H.E.V. Brown, J. Osborne, R. Axel, and J.A. Gogos. 2004. Spontaneous neural activity is required for the establishment and maintenance of the olfactory sensory map. *Neuron.* 42:553–566. http://dx.doi.org/10.1016/S0896-6273(04)00224-7

Zhainazarov, A.B., and B.W. Ache. 1995. Odor-induced currents in *Xenopus* olfactory receptor cells measured with perforated-patch recording. *J. Neurophysiol.* 74:479–483.

Zhao, H., L. Ivic, J.M. Otaki, M. Hashimoto, K. Mikoshiba, and S. Firestein. 1998. Functional expression of a mammalian odorant receptor. *Science.* 279:237–242. http://dx.doi.org/10.1126/science.279.5348.237

Zheng, C., P. Feinstein, T. Bozza, I. Rodriguez, and P. Mombaerts. 2000. Peripheral olfactory projections are differentially affected in mice deficient in a cyclic nucleotide-gated channel subunit. *Neuron.* 26:81–91. http://dx.doi.org/10.1016/S0896-6273(00)81140-X